



Norwegian University of
Science and Technology

TMR4520

PROJECT MASTER THESIS

TOWARDS THE HYDRODYNAMIC STUDY OF A 2D FISH-LIKE
GEOMETRY DURING LOCOMOTION

JONATHAN DAVID LAURITZEN SCHWARTZ

July 1, 2019



MASTER THESIS IN MARINE TECHNOLOGY

Spring 2019

FOR

Jonathan David Lauritzen Schwartz

Hydrodynamic Study of a 2D Fish-like geometry during Locomotion

(Hydrodynamisk studie av en 2D geometri lik fisk under bevegelse)

Fish and mammals can be marine vehicles with high hydrodynamic efficiency. Some of them are able to use their compliant skin, their mucus, or their skin micro and macro features to reduce the frictional stresses along their wetted surface or to limit/suppress vortex shedding from their body. These aspects can reduce the resistance experienced by the animal and some of them can improve the steering performances.

A preliminary project work has been carried out to document the state of the art and to identify some relevant reference studies. The open-source CFD platform OpenFOAM was selected as numerical tool for the research and applied to the test case of a rigid foil, in infinite liquid, interacting with a steady inflow with angle of attack.

Objective

The present master thesis aims to investigate numerically selected fish mechanisms to enhance efficiency during locomotion. The focus will be on sub-carangiform fish locomotion. The study will be carried out as an in-depth and systematic parameter analysis through examining a 2D fish-like geometry in infinite liquid.

The work should be carried out in steps as follows:

1. Summarize major findings/outcomes from the project thesis and complement the literature survey in order to identify state-of-the-art of the problem. Provide an overview of relevant non-dimensional parameters identified. The emphasis should be on sub-carangiform fish locomotion and on the numerical methods used to handle body flexibility.
2. Describe the numerical method selected as research tool and its basic assumptions. Perform a systematic study to overcome the grid-generation issues, faced during the project work, in the case of a rigid foil in a steady current with angle of attack.
3. Use the relevant reference results identified in literature study, to verify/validate the numerical method for a simplified 2D rigid foil in forced oscillatory motion (heave/pitch). Examine motion conditions that bring from a drag to a thrust of the fish because of changes in the wake features. Perform a numerical-convergence analysis if time allows.
4. If time allows, use the relevant reference results identified in literature study, to verify/validate the numerical method for a simplified 2D flexible foil in forced motion and to carry on a systematic analysis of kinematic and dynamic flow features when the body locomotion involves flexible motions.
5. Draw the conclusions from the studies and discuss possible further steps in the numerical investigation of fish locomotion.

The work may show to be more extensive than anticipated. Some topics may therefore be left out after discussion with the supervisor without any negative influence on the grading.

The candidate should in his report give a personal contribution to the solution of the problem formulated in this text. All assumptions and conclusions must be supported by mathematical models and/or references to physical effects in a logical manner.

The candidate should apply all available sources to find relevant literature and information on the actual problem.

The thesis should be organized in a rational manner to give a clear presentation of the work in terms of exposition of results, assessments, and conclusions. It is important that the text is well written and that tables and figures are used to support the verbal presentation. The thesis should be complete, but still as short as possible. In particular, the text should be brief and to the point, with a clear language. Telegraphic language should be avoided.

The thesis must contain the following elements: the text defining the scope (i.e. this text), preface (outlining project-work steps and acknowledgements), abstract (providing the summary), table of contents, main body of thesis, conclusions with recommendations for further work, list of symbols and acronyms, references and (optional) appendices. All figures, tables and equations shall be numerated.

The supervisor may require that the candidate, in an early stage of the work, present a written plan for the completion of the work. The plan should include budget for the use of computer and laboratory resources that will be charged to the department. Overruns shall be reported to the supervisor.

From the thesis it should be possible to identify the work carried out by the candidate and what has been found in the available literature. It is important to give references to the original source for theories and experimental results.

Supervisor : Marilena Greco
Co-supervisor : Claudio Lugni

Submitted : January 15th 2019
Deadline : June 11th 2019

Marilena Greco
Supervisor

1 Acknowledgements

I would like to thank my supervisor Professor Marilena Greco and my co-supervisor Adjunct Professor Claudio Lugni for their precious advices all this semester and also Phd-students Hui-li Xu and Mohd Atif Siddiqui for their great help.

2 Preface

During the master thesis a NACA0012 foil has been studied in Openfoam in static cases and with fish-like locomotion to study the effects on the propulsion of a fish. The main challenge during this thesis was to find a good grid strategy to use for the simulations in Openfoam. Finding the right grid and the right strategy in Openfoam has been very time-consuming and represents most of the thesis in terms of work amount.

3 Abstract

This master thesis presents the results of simulations done with a NACA0012 foil for static cases and for a subcarangiform fish-like motion. The preliminary study was to analyze the results given by Openfoam on a static NACA0012 foil in order to obtain similar results to the literature. This first stage was to validate the model used in Openfoam. The first strategy was using a deformable grid. The grid is a rectangle domain made in ICEM. The points of the foil were then rotated at the desired angle. This way of making the foil rotate stretched the cells. In consequence the results were not good enough and then rejected. Next, a strategy of overset grid was used in Openfoam, first with three grids. A bodyfitted grid for the foil made in ICEM, a refinement grid and a background grid. The purpose of the refinement grid was to make the transition of the cell size between the bodyfitted grid and the background grid smooth and then to avoid too many cells in total. Once more this strategy didn't give satisfying results. A discontinuity which was not visible in the first place was discovered in Paraview using the threshold function. Finally, an overset grid was tested with only a bodyfitted grid and a background grid. This strategy gave good results. A convergence analysis was then conducted to choose a grid for the fish-like motion. The final study comprises several simulations with expected formation of reversed BvK vortex street typically produced by fishes. First a simulation combining heave and pitch was tested for phase shift $\psi = 90^\circ$ and $\psi = 10^\circ$. The first one was expected to give thrust and the second less thrust or drag. Both produced drag. In order to find out the reason why no thrust was produced a more simple motion was tested with a pitching foil. The simulation of a pitching foil was tested with the selected grid of the convergence study. The simulation didn't produce thrust as it was expected. The model used in Openfoam has shown good results for static simulations but was not convincing for motion simulations. The results of this thesis suggest that the overset grid doesn't work well for motions with a small bodyfitted grid around the foil and the use of one or several refinement grids between the foil and the background grid should be tested. Previous tests have shown that the last suggestion doesn't work when the calculations are decomposed in the supercomputer. These results show the limitations of Openfoam and suggest that more in depth investigations about the use of overset grid and the use of supercomputer should be done. It is also suggested that the next investigations should use a much wider bodyfitted grid with unstructured cells. The cells around the foil should be much finer than the previous study and progressively expanded until the boundary of the bodyfitted grid in order to keep the cell size in the background grid bigger and reduce the running time.

4 Sammendrag

Denne masteroppgaven viser resultater fra simuleringer av en NACA0012 foil i statiske og bevegelige tilfeller. En innledende studie har hatt som formål å simulere en statisk foil og å få til resultater tilsvarende det som finnes i litteraturen. Dette for å bekrefte at modellen i Openfoam er pålitelig. Første forsøk besto av å bruke et firkantet rutenett laget i ICEM med en foil som hadde angrepsvinkel lik 0. Koordinatene av foilen ble deretter rotert ved hjelp av Openfoam til ønsket angrepsvinkel. Dette gjorde at enkelte celler ble strukket og resultatene var ikke tilfredsstillende. Neste strategi var å bruke en "overset grid" i Openfoam som er et rutenett som beveger seg på et bakgrunnsrutenett. Dette systemet besto av tre forskjellige rutenett. Et var brukt som formtilpasset til foilen, et annet var brukt som bakgrunn og et tredje som overgang mellom de to førstnevnte. Overgangsruutenettet var tenkt for å få en myk overgang mellom de to andre og i tillegg å unngå altfor mange celler totalt. Denne strategien var heller ikke tilfredsstillende og ga dårlige resultater. Det ble oppdaget en diskontinuitet ved hjelp av Paraview og threshold-funksjonen mellom foil-rutenettet og overgangsruutenettet. Til slutt ble den samme simuleringen gjort med bare foil-rutenettet og bakgrunnsrutenettet og resultatene ble tilfredsstillende. Deretter ble en konvergenstudie utført for å velge den beste løsningen til neste simulering med bevegelse. Neste studie simulerte en foil med både hiv- og stampbevegelse. Målet var å kunne observere reversert BvK virvelbevegelse som er typisk for fisk. Simuleringen ble gjort for fasevinkel $\psi = 90^\circ$ og $\psi = 10^\circ$. Førstnevnte var forventet å produsere skyvekraft, mens den andre var forventet å produsere motstand eller mindre skyvekraft. Begge tilfellene viste seg å produsere motstand og BvK virvelbevegelse. Til slutt ble en foil med stampbevegelse simulert i Openfoam. Denne ble testet med samme rutenett som det som ble valgt under konvergenstudien. Simuleringene gav heller ikke tilfredsstillende resultater. Modellen brukt i Openfoam har vist seg å være god til å simulere statiske tilfeller, men viste begrensninger når det gjaldt å simulere en bevegelig foil. Resultatene fra denne masteroppgaven viser at overset grid ikke fungerer med et lite formtilpasset rutenett rundt foilen og at bruk av ett eller flere overgangsruutenett burde brukes. Tidligere simuleringer har vist at bruk av overgangsruutenett ikke fungerer når beregningene er oppdelt med superdatamaskinen. Disse resultatene viser begrensningene til Openfoam og foreslår at mer detaljerte undersøkelser må gjøres ved bruk av overset og superdatamaskinen. Det er også foreslått at neste undersøkelse burde prøve foil-rutenettet som er mye større med ustrukturert celler. Nær foilen burde cellene være mye mindre enn i de forrige simuleringene og expanderes frem til grensen til foil-rutenettet, noe som vil kunne tillate større celler i bakgrunnsruutenettet og dermed redusere simuleringstiden.

Contents

1	Acknowledgements	
2	Preface	
3	Abstract	
4	Sammendrag	
5	Introduction	1
6	Preliminary work	2
6.1	Introduction and overview of the swimming modes	2
6.2	Parameters of the subcarangiform swimming mode	3
6.3	Numerical studies on swimming modes	6
7	Openfoam	8
8	Static foil study with stretchable grid	9
8.1	Assumptions in Openfoam	9
8.2	Rectangular grid	10
8.3	Moving points	12
8.3.1	Velocity plot in Paraview	14
8.3.2	Comparison of drag and lift coefficient	15
8.3.3	Pressure coefficient plot	16
8.3.4	Velocity at 20% and 80 % of chord length	18
8.4	Overset grid	20
8.4.1	Assumptions in Openfoam	20
8.4.2	Strategy	21
8.5	Boundary fitted grid	22
8.5.1	Entire grid	23
8.5.2	Refinement zone	24
8.5.3	Drag and lift coefficient	25
8.5.4	Comparison of drag and lift coefficients	26
8.5.5	Discontinuity between grids	27
8.6	Convergence study	29
8.6.1	Improved bodyfitted grid	29
8.6.2	Domain convergence study	30
8.6.3	Cell size convergence study	35
8.6.4	Domain convergence study	39

8.6.5	Flow features	42
9	Heaving and pitching foil	45
9.1	Heave and pitch equations	45
9.1.1	Parameters for the rigid motion of the foil	45
9.1.2	Calculation of thrust produced	45
9.2	Vorticity during one period for $\psi = 90$	47
9.3	Vorticity during one period for $\psi = 10$	49
9.4	Drag coefficient on the body	51
9.5	Comparison of velocity field with Anderson et al.	53
9.6	Pitching foil	57
10	Discussion and further work	59
11	Conclusion	60

List of Figures

1	(a) anguilliform mode, (b) carangiform mode, (c) subcarangiform mode, (d) thunniform mode. Figure taken from Lane et al. [5]	3
2	Motion of the fish described by the lateral excursion of the body $h(x,t)$, the velocity of the fish U and the wave velocity V . The figure is taken from Cui et al. [19]	4
3	Adult (A) and juvenile (A) fishes. Figure taken from Archer et al. [2]	5
4	Rectangle grid made in ICEM	10
5	Leading edge	11
6	Trailing edge	12
7	10° rotation of the foil in Openfoam	13
8	Velocity plot for $Re = 5000$ and $AOA = 10^\circ$	14
9	Final drag and lift coefficient compared with Razavi et al. [17]	15
10	Pressure coefficient compared with Hafez et al. Results taken from Razavi et al. [17]	16
11	U magnitude for minimum lift [ms^{-1}]	17
12	Pressure at minimum lift [m^2s^{-2}]	17
13	Vorticity at minimum lift [s^{-1}]	17
14	Comparison for $Re = 2000$ and $AOA = 0^\circ$ with Pascazio and Napolitano, results taken from Razavi et al. [17]	18
15	Comparison for $Re = 2000$ and $AOA = 0^\circ$ with Pascazio and Napolitano, results taken from Razavi et al. [17]	19
16	U magnitude for minimum lift ms^{-1}	20
17	Pressure at minimum lift [m^2s^{-2}]	20
18	Vorticity at minimum lift [s^{-1}]	20
19	Body-fitted Grid	22
20	Entire domain seen in Paraview	23
21	Refinement zone	24
22	Drag and lift coefficients versus time for $Re 5000$ and $AOA = 5^\circ$	25
23	Final drag and lift coefficient compared with Razavi et al. [17]	26
24	View of the body fitted grid and refinement grid	27
25	Boundary region between bodyfitted grid and refinement grid	28
26	Boundary region between refinement grid and background grid	28
27	Period of drag function of domain size	29
28	Discontinuity in the vorticity	29
29	Improved bodyfitted grid	30
30	Threshold	31
31	C_p for all the cases	31
32	C_p for medium cell size against Kurtulus	32
33	C_p for finest cell size against Kurtulus	32

34	Lift coefficient	33
35	Drag coefficient	34
36	Mean drag function of number of cells along the foil	37
37	Mean lift function of number of cells along the foil	37
38	RMS of drag function of number of cells along the foil	37
39	RMS of lift function of number of cells along the foil	37
40	RMS of drag function of number of cells along the foil	38
41	RMS of lift function of number of cells along the foil	38
42	Mean drag function of domain size	40
43	Mean lift function of domain size	40
44	RMS of drag function of domain size	40
45	RMS of lift function of domain size	40
46	Period of drag function of domain size	41
47	Period of lift function of domain size	41
48	U magnitude for maximum lift [ms^{-1}]	42
49	Pressure at maximum lift [m^2s^{-2}]	42
50	Vorticity at maximum lift [s^{-1}]	42
51	U magnitude between maximum and minimum lift [ms^{-1}]	43
52	Pressure between maximum and minimum lift [Nm^{-2}]	43
53	Vorticity between maximum and minimum lift [s^{-1}]	43
54	U magnitude for minimum lift [ms^{-1}]	44
55	Pressure at minimum lift [Nm^{-2}]	44
56	Vorticity at minimum lift [s^{-1}]	44
57	t = 3 s	47
58	t = 3.0248 s	47
59	t = 3.05 s	47
60	t = 3.0748 s	47
61	t = 3.108 s	47
62	t = 3.1244 s	47
63	t = 3.1496 s	48
64	t = 3.1744 s	48
65	t = 3.216 s	48
66	t = 3.224 s	48
67	t = 3.2492 s	48
68	t = 3 s	49
69	t = 3.0248 s	49
70	t = 3.05 s	49
71	t = 3.0748 s	49

72	t = 3.108 s	49
73	t 3.1244 s	49
74	t = 3.1496 s	50
75	t = 3.1744 s	50
76	t = 3.216 s	50
77	t = 3.224 s	50
78	t = 3.2492 s	50
79	Drag coefficient for $\psi = 90$	51
80	Drag coefficient for $\psi = 10$	51
81	Drag producing vortex Picture taken from Jones et al. [13]	51
82	Thrust producing vortex Picture taken from Jones et al. [13]	51
83	Velocity profile behind the foil for $\psi = 90^\circ$	52
84	Velocity profile behind the foil for $\psi = 10^\circ$	52
85	Velocity field at left taken from Anderson et al. [12] and Openfoam (right). The pictures are taken from one half period with dimensionless time step $\Delta t = 0.042$	56
86	Screenshot from the vorticity at t = 9.9365 s	57
87	Velocity field from the entire domain at t = 9.9365 s	57
88	Spanwise vorticity (left) and mean flow (right) from Godoy-Diana et al. Picture taken from Godoy-Diana [10]	57
89	Drag coefficient for the flapping foil	58

List of Tables

1	Kinematics of burst swimming. Data taken from Archer et al. [2]	5
2	Boundary conditions	9
3	Boundary conditions	21
4	Drag and lift coefficients compared with Kurtulus [14]	27
5	Parameters of the different cases and results for C_D and C_L	30
6	Parameters and results of the cell size convergence study	35
7	Order of accuracy for the cell size convergence study	36
8	Parameters used for the OA analysis	36
9	Parameters and results for the domain size convergence study	39

Nomenclature

δ	Boundary layer thickness
λ	Wave length
ν	Kinematic viscosity
ψ	Phase shift between heave and pitch
A	Wide of the wake
$a(Z)$	Amplitude envelope from the lateral motion
BCF	Body and/or Caudal Fin
BvK	Bénard-von Kármán
c	Chord length of the foil
C_D	Drag coefficient
C_L	Lift coefficient
C_P	Pressure coefficient
COD	Complex Orthogonal Decomposition
f	Tail-beat frequency
h	Amplitude of heaving
$h(z, t)$	Lateral excursion of the body
k	Wave number
L	Length of the foil
MPF	Median and/or Paired Fin
Re	Reynolds number
RMS	Root mean square
St	Strouhal number
U	Inline velocity

5 Introduction

To design our constructions the best inspiration often comes from the nature itself. The evolution has permitted some animals to become very efficient, using as less as possible energy with very high speed for instance. In the marine industry we are looking for reducing or no fuel consumption. By studying the way fishes move in the water, new solutions could maybe give better designs for our marine vessels. The subcarangiform swimming seems to be one of the less studied type of fish locomotion. The purpose of this master thesis is to study the effects of this type of swimming on a rigid body like the NACA0012 foil. The thesis is divided into the following main parts: First part is a literature study presenting an overview of the different swimming modes and a description of the subcarangiform swimming mode. Next, numerical studies for a static NACA0012 foil are presented and finally, a study of a moving NACA0012 foil imitating subcarangiform swimming mode is presented.

6 Preliminary work

6.1 Introduction and overview of the swimming modes

The swimming mechanism of fishes can be divided in two main swimming modes (Lane et al. [5]): The Body and/or Caudal Fin (BCF) movement and the Median and/or Paired Fin (MPF). The MPF is usually employed for low speed while BCF swimming is used for great thrust and acceleration. The BCF swimming mode can then be divided into two sub-modes: undulatory and oscillatory. In order to reduce the scope of this project, the focus will be on BCF-undulatory swimming mode which can be classified in anguilliform, subcarangiform, carangiform and thunniform mode. Two methods are used to describe these swimming modes: the lift-based method used for thunniform swimming and the added-mass method used for anguilliform, subcarangiform and carangiform swimming. The added-mass method can be explained like this: there is a propulsive wave passing backwards that goes along the fish and each segment of the fish contributes to increasing the momentum of this propulsive wave. The water reacts then with an opposing force F_R on the body of the fish. This force is equal to the accelerated mass of the water times the acceleration of the water (Lane et al. [5]). This force can be divided into a lateral and a thrust component. For anguilliform motion the entire body contributes to the thrust with large-amplitude undulations. The subcarangiform swimming uses the same technique but only the half part is undulating. For carangiform swimmers the undulations are done by one third at the end of the body length. The carangiform swimmers have also a stiffer caudal fin allowing them to swim faster than anguilliform and subcarangiform fishes, but have less manoeuvrability. Carangiform swimming has also more risks of recoil because the lateral forces are concentrated at the end of the body. Finally, the thunniform mode generates thrust by the lift-based method. About 90% of the thrust comes from the caudal fin which is very stiff and high. The streamlined body of the fish allows to reduce pressure drag. Furthermore, recoil is avoided because of the body shape and the mass distribution. These features make the thunniform mode as the most efficient swimming mode.

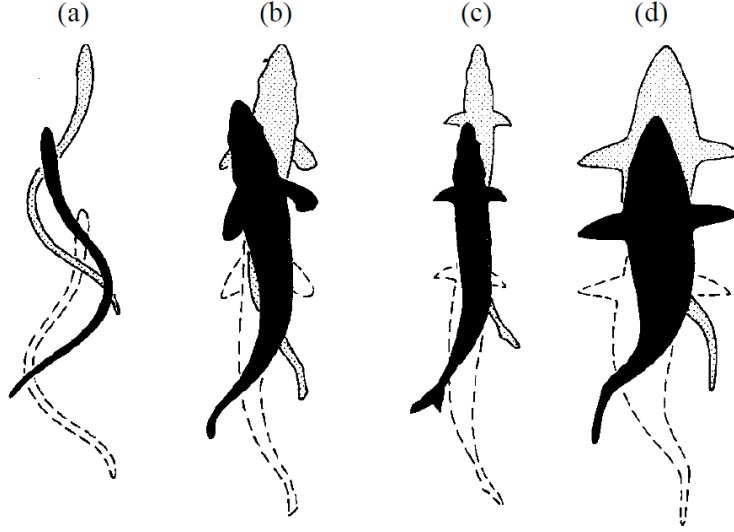


Figure 1: (a) anguilliform mode, (b) carangiform mode, (c) subcarangiform mode, (d) thunniform mode. Figure taken from Lane et al. [5]

6.2 Parameters of the subcarangiform swimming mode

To perform simulations reproducing the subcarangiform swimming it is necessary to study the characteristics of this swimming mode and define the parameters that can be defined in a CFD solver. The main parameters relevant for the motion of a fish are the Reynolds number and the Strouhal number.

$$Re = \frac{U}{\nu L} \quad (1)$$

The Reynolds number tells if the motion of the fish is turbulent or laminar. For subcarangiform fishes, the range is $10^4 < Re < 10^6$ (Lane et al. [5]). U is the inline velocity [ms^{-1}], ν is the kinematic viscosity [ms^{-2}] and L [m] the length of the fish. The Strouhal number is given by the following formula.

$$St = \frac{fA}{U} \quad (2)$$

A represents the width of the wake which is the maximum lateral excursion [m], f is the tail-beat frequency and U the inline velocity of the fish. It tells how many vortices are created by unit time in the flow behind the fish. For subcarangiform fishes the Strouhal number lies in a range of $0.25 < St < 0.40$ (Lane et al. [5]).

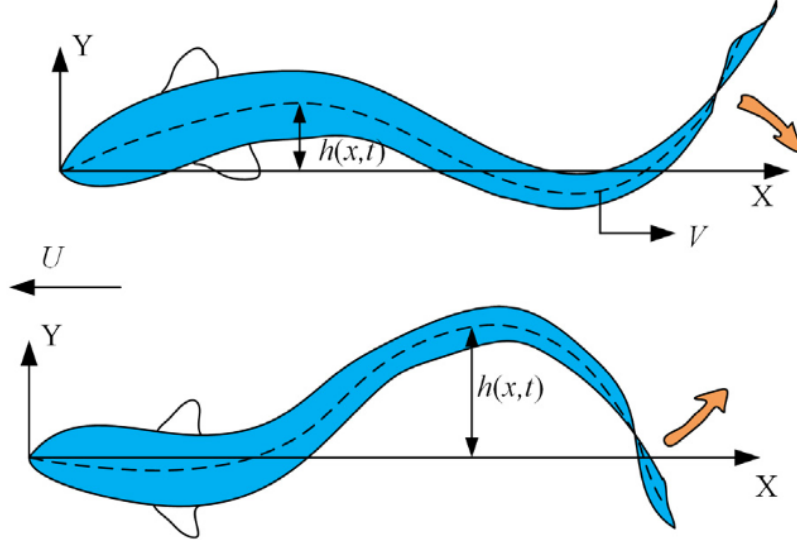


Figure 2: Motion of the fish described by the lateral excursion of the body $h(x,t)$, the velocity of the fish U and the wave velocity V . The figure is taken from Cui et al. [19]

The locomotion of a fish can be described with the following equation that represents the lateral excursion of the body at time t (Borazjani et al. [11]).

$$h(x, t) = a(x)\sin(kx - \omega t) \quad (3)$$

where $a(x)$ is the amplitude envelope from the lateral motion, k the wave number which depends on the wave length $k = \frac{2\pi}{\lambda}$, $\omega = \frac{2\pi}{f}$ is the angular frequency and f the tail-beat frequency [s^{-1}]. The amplitude envelope from the lateral motion $a(x)$ varies for each type of swimming mode. For the subcarangiform mode Cui. et al. [19] defines it like:

$$a(x) = a_1 + a_2x + a_3x^2 = s_2L - \frac{2s_4(s_3 - s_2)}{1 - 2s_4}x - \frac{s_3 - s_2}{(1 - 2s_4)L}x^2 \quad (4)$$

Cui. et al. [19] has listed many types of fishes in a table as the rainbow trout. For this fish equation 4 becomes

$$a(x) = \frac{s_3}{L}x^2 = \frac{0.12}{L}x^2 \quad (5)$$

The wavelength for the rainbow trout is comprised between 0.7 m and 1.3 m. The tail-beat frequency is in a range between 4 and 11 Hz. If we take $\lambda = 1$ m and $f = 7.5$ Hz, the equation of lateral excursion of the fish becomes

$$h(x) = \frac{0.12}{L}x^2\sin(2\pi x - (2\pi \cdot 7.5)t) \quad (6)$$

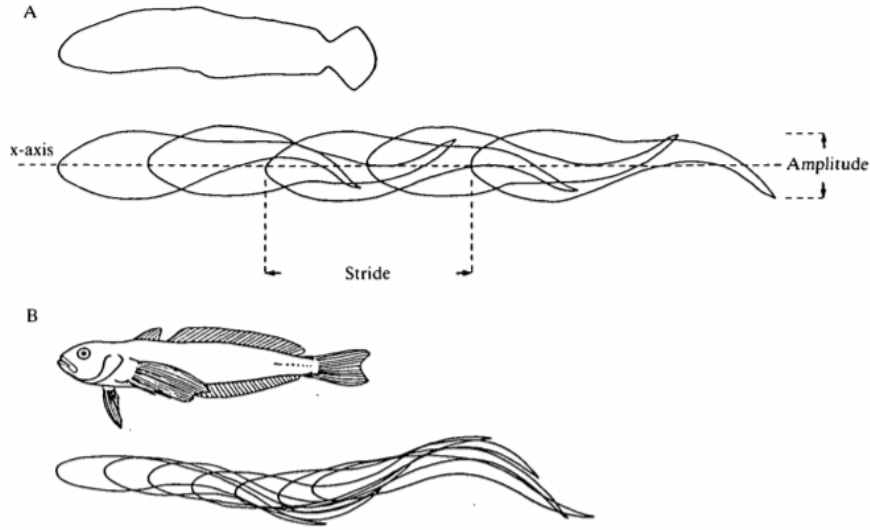


Figure 3: Adult (A) and juvenile (A) fishes. Figure taken from Archer et al. [2]

Figure 3 and table 1 present some swimming characteristics of a subcarangiform fish, the *notothenia neglecta*. The swimming mode of the *notothenia neglecta* has been studied for adult and juvenile by Archer et al. [2]. The fishes were caught in the South Orkney Islands and transported to Scotland and placed in special tanks to observe their swimming mode. Stride, tail-beat frequency, amplitude and speed were measured. Subcarangiform swimming was used at the following speed and tail-beat frequencies (see table 1). For adults (27-30 cm) the tail-beat frequency was of the range of 5.0-8.3 Hz and the speed was of the range of 3.6-5.4 $L.s^{-1}$ where L is the length of the fish. For juvenile (7-8 cm) the tail-beat frequency was between 4.0-12.5 Hz and the speed of the range 2.3-8 $L.s^{-1}$. In table 1 the results of burst swimming can be seen.

Table 1: Kinematics of burst swimming. Data taken from Archer et al. [2]

Fish (cm)	Velocity (Ls^{-1})	Velocity (cms^{-1})	Tail-beat frequency (Hz)	Tail-beat amplitude (L)	Stride length (L)
Adults fish					
30.5	4.2 ± 0.2	128 ± 5.8	6.3 ± 0.2	0.20 ± 0.02	0.67 ± 0.05
29.5	4.2 ± 0.3	127 ± 9.8	6.1 ± 0.8	0.19 ± 0.04	0.70 ± 0.04
26.9	4.7 ± 0.5	127 ± 12.5	7.1 ± 0.9	0.21 ± 0.03	0.67 ± 0.06
30.2	4.1 ± 0.4	123 ± 11.6	6.9 ± 0.2	0.18 ± 0.02	0.59 ± 0.06
Mean (L)					
29.3 ± 1.6	4.3 ± 0.4	126 ± 9.7	6.6 ± 0.6	0.20 ± 0.03	0.66 ± 0.06
Juvenile					
8.1	6.2 ± 1.0	50 ± 7.8	10.0 ± 1.5	0.27 ± 0.01	0.63 ± 0.13
7.9	6.7 ± 1.0	53 ± 8.2	8.3 ± 0.9	0.29 ± 0.03	0.81 ± 0.12
7.2	6.8 ± 0.4	49 ± 3.3	8.2 ± 1.2	0.29 ± 0.04	0.83 ± 0.07
7.1	7.4 ± 1.3	53 ± 9.7	9.1 ± 1.5	0.31 ± 0.05	0.82 ± 0.12
Mean(L)					
7.6 ± 0.5	6.8 ± 1.0	51 ± 7.2	8.9 ± 1.4	0.29 ± 0.04	0.77 ± 0.14

The kinematics of swimming of the subcarangiform mode has also been studied by Cui et al. [19]. The study concluded that subcarangiform swimming could be described by the mixed motion composed of standing and travelling waves. The travelling index of subcarangiform fish was found to be in a range of 0.52-0.78. The travelling index is defined as the relative ratio between the magnitudes of the travelling and standing components of the midline motions (definition taken from Cui et al. [19]). The study has also listed biological data about subcarangiform fishes such as the amplitude, the tail-beat frequency and the wave number of the midline motion.

The work of Eloy [6] presents the swimming kinematics of 53 species of aquatic animals with length, surface ratio, Reynolds number, Lighthill number, Strouhal number, the slip ratio and the maximum incident angle. By collecting these data, the study has shown that the Strouhal number of these animals were in the same range than the one used in experiments with flapping foils with maximum propulsive efficiency.

The literature gives us a lot of information about the characteristics of the subcarangiform mode. This will be used to make equations describing a fish-like rigid body motion with a foil in Openfoam.

6.3 Numerical studies on swimming modes

To understand swimming modes, experimental and numerical studies on fishes have been made. This has for instance been studied by Maertens et al. [3] with a study on undulating swimming fishes. A single fish-like body and a pair of swimmers were simulated. The main parameters used were the Strouhal number, the phase angle between heave and pitch at the trailing edge and the angle of attack. The simulations were made for carangiform swimming at $Re = 5000$. The efficiency of one single fish swimming alone and interacting fishes was calculated.

Numerical methods have been used by Borazjani et al. [11] to study the body shape and kinematics on the hydrodynamics for carangiform and anguilliform swimmers. The study used the hybrid Cartesian immersed-boundary method. This study showed that anguilliform mode was more efficient than carangiform in the viscous ($Re \approx 10^2$) and transitional regime ($Re \approx 10^3$) whereas carangiform was more efficient than anguilliform mode in inertial regime ($Re \approx \infty$). Cui et al. [19] studied undulating swimming BCF mode. The midline motions of the fish were decomposed into travelling and standing components. The method of complex orthogonal decomposition (COD) was used to analyze the midline motion. The study classified the subcarangiform and carangiform in a new category. Subcarangiform and carangiform fishes use a mixture wave form combining the standing-wave and travelling-wave form. Schultz et al. [18] have studied the energy consumption and swimming of carangiform, anguilliform and thunniform modes with 2D models using CFD. All these studies show that studying the swimming modes is a very large field and after have been through this literature it is suggested for this thesis to focus on and analyze in more detail the subcarangiform mode. The study in the thesis will focus on the rigid body fish-like motion of a moving foil. Several studies using devices such as flapping foils have also been made in order to understand the mechanism of swimming of fishes. For instance, Schouveiler et al. [15] have analyzed the effect of changing the

Strouhal number and the angle of attack for flapping foil on thrust and hydromechanical efficiency. This experimental study was based on thunniform swimming. Experimental studies were also compared to numerical results on flapping foils by Anderson et al. [12] where the importance of the phase angle between heave and pitch was highlighted. Godoy-Diana et al. [10] studied the vortex in the wake of a pitching foil to study the transition between Bénard-von Kármán (BvK) to reversed BvK vortex street.

7 Openfoam

This section intends to give a quick overview of how an Openfoam case is used. An Openfoam folder contains generally three subfolders. The points below describe the main function of each of these subfolders.

- System

This is the main folder which coordinates all the subfolders in a case. It controls the main parameters of the simulation such as the Openfoam solver, the time step, start time and end time and the values to write as output.

- Constant

This folder contains the information about the grid, the turbulence and transport properties and how the foil is behaving.

- 0

This folder contains the boundary conditions of the velocity and the pressure at the boundary of the domain and around the foil.

8 Static foil study with stretchable grid

8.1 Assumptions in Openfoam

In this section the solver PISO is used for the simulations of a NACA0012 foil in a laminar flow (Re 500, 2000 and 5000). The PISO solver is transient and suited for incompressible and turbulent flow using the PISO algorithm [1]. PISO stands for Pressure Implicit with Splitting of Operators. The turbulence mode can be turned off and changed to laminar model. The characteristics of the PISO model correspond well to the flow characteristics this section will study.

Table 2: Boundary conditions

BC	Inlet	Outlet	Foil	Top and bottom	Front and back
P	Zero gradient	Fixed value = uniform 0	Zero gradient	Zero gradient	Empty
U	Uniform value table	Zero gradient	Uniform(0,0,0)	Zero gradient	Empty

The boundary conditions have been summarized in table 2. The BC for front and back planes are set to empty since this is a 2D simulation. The velocity on the foil is defined as Uniform(0,0,0) which means no slip. The pressure on the foil is defined as zero gradient because this is a wall. At the inlet the velocity is set to uniform value table to make the velocity increase progressively to (1,0,0) to avoid too high CFL number at the beginning, this is a ramp function. The pressure at the inlet is set to zero gradient because the pressure is constant. At the outlet the velocity is set to zero gradient because there is no change in velocity. The pressure is zero at the outlet. On the top and bottom of the domain the velocity and pressure are constant in order not to disturb the flow. This is therefore defined in Openfoam as zero gradient.

8.2 Rectangular grid

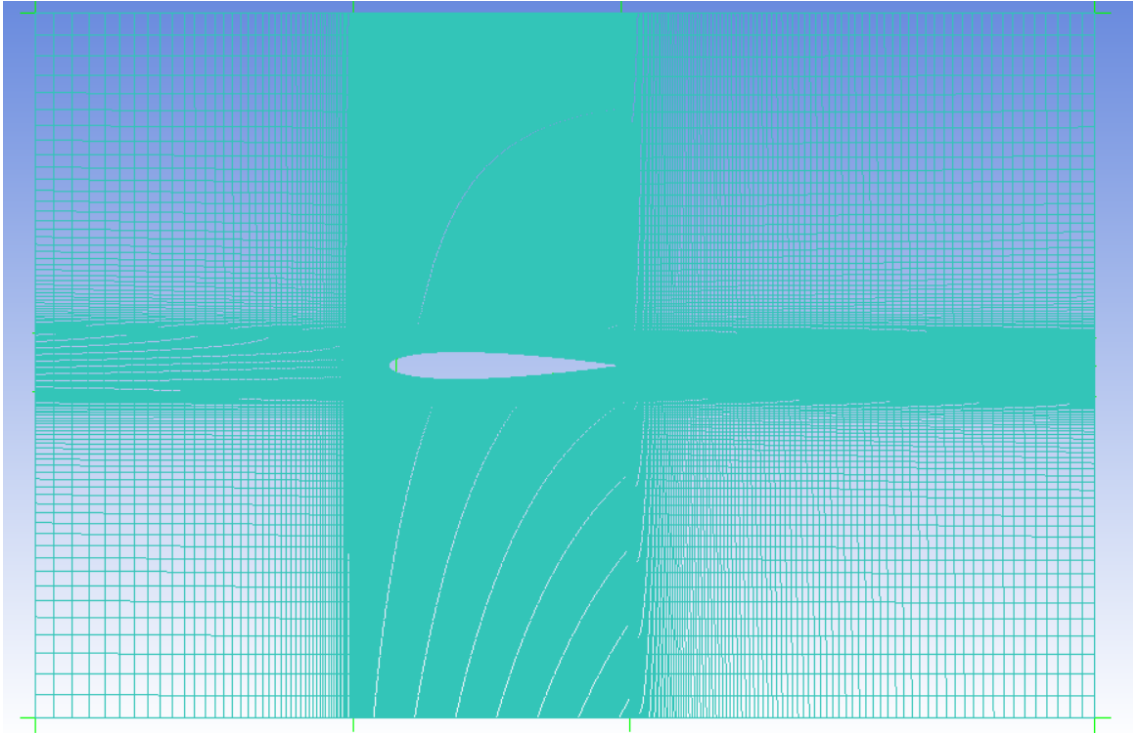


Figure 4: Rectangle grid made in ICEM

The software ICEM was used to make a new grid inspired from Esmailifara et al. [7] with a NACA0012 foil with zero angle of attack. The main challenge when making a grid for the NACA0012 foil is to have cells that are perpendicular all along the body and at the same time ensure uniformity in the domain. Figure 4 shows the rectangle grid. The drawback with this method is that we get a very fine cell size in the entire length in horizontal and vertical direction of the foil, this looks like a cross. Often, the main issue is at the leading edge where the cell size is expanding and then making the cells much wider in front of the foil than on each side of the foil. A compromise for the cell size at the leading edge has to be found to avoid singularities in the domain. Figure 5 shows the cell size around the leading edge. It can easily be seen that the cell size is not perfectly uniform.

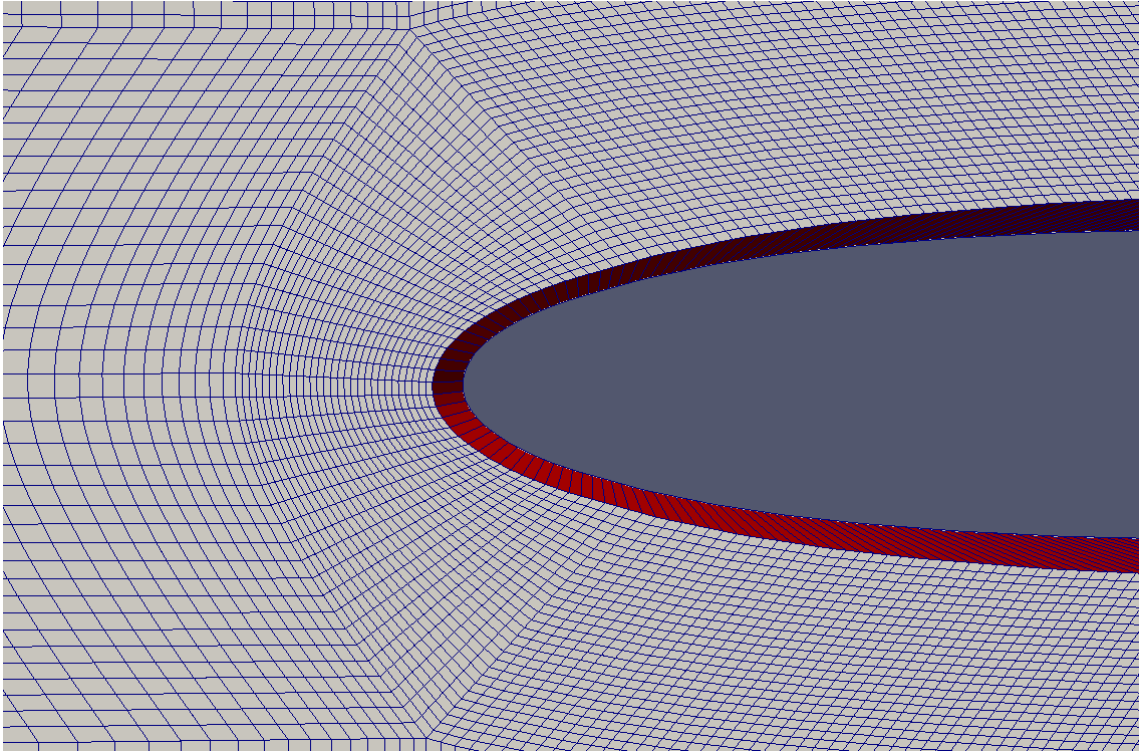


Figure 5: Leading edge

Figure 5 shows the cell size at the leading edge of the foil.

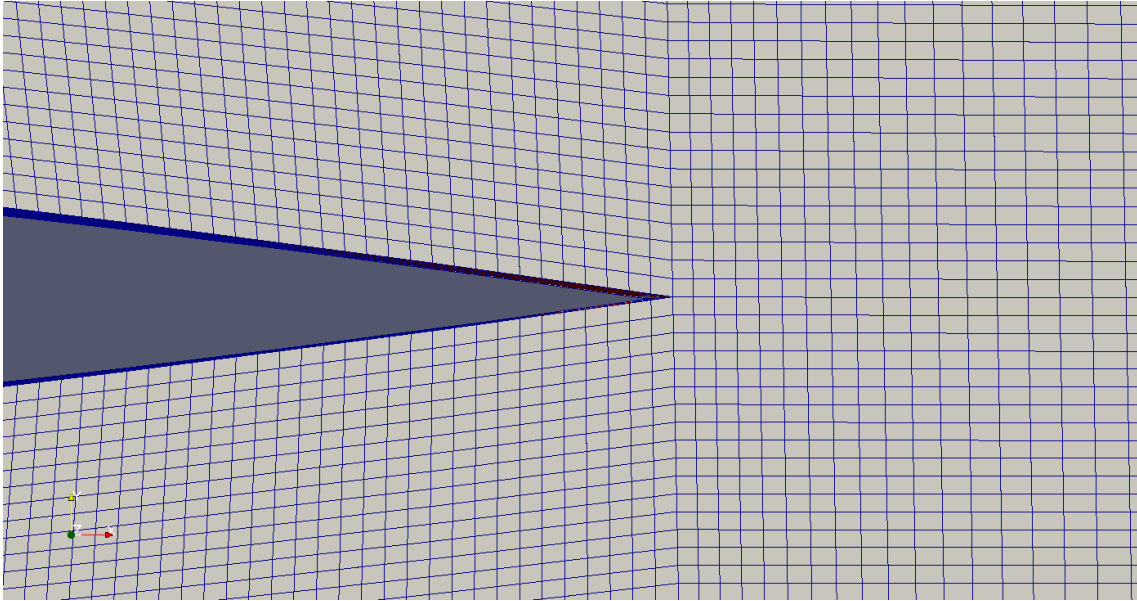


Figure 6: Trailing edge

At the trailing edge the cell size is uniform everywhere as it can be seen in figure 6.

8.3 Moving points

After having made a grid for the foil at zero angle of attack, the idea was to rotate it in Openfoam with point displacements. This operation permits to rotate the foil at the desired angle of attack and then extract the grid which corresponds to a certain angle of attack. Thus, instead of making a new grid for each angle attack only one is needed. In a folder called point displacement the foil was given a certain amplitude and oscillating rotation and stopped at the desired angle of attack. This strategy makes the cells move in the grid and result to stretching of the cells. Figure 7 shows an example about a foil that is rotated to 10° angle of attack.

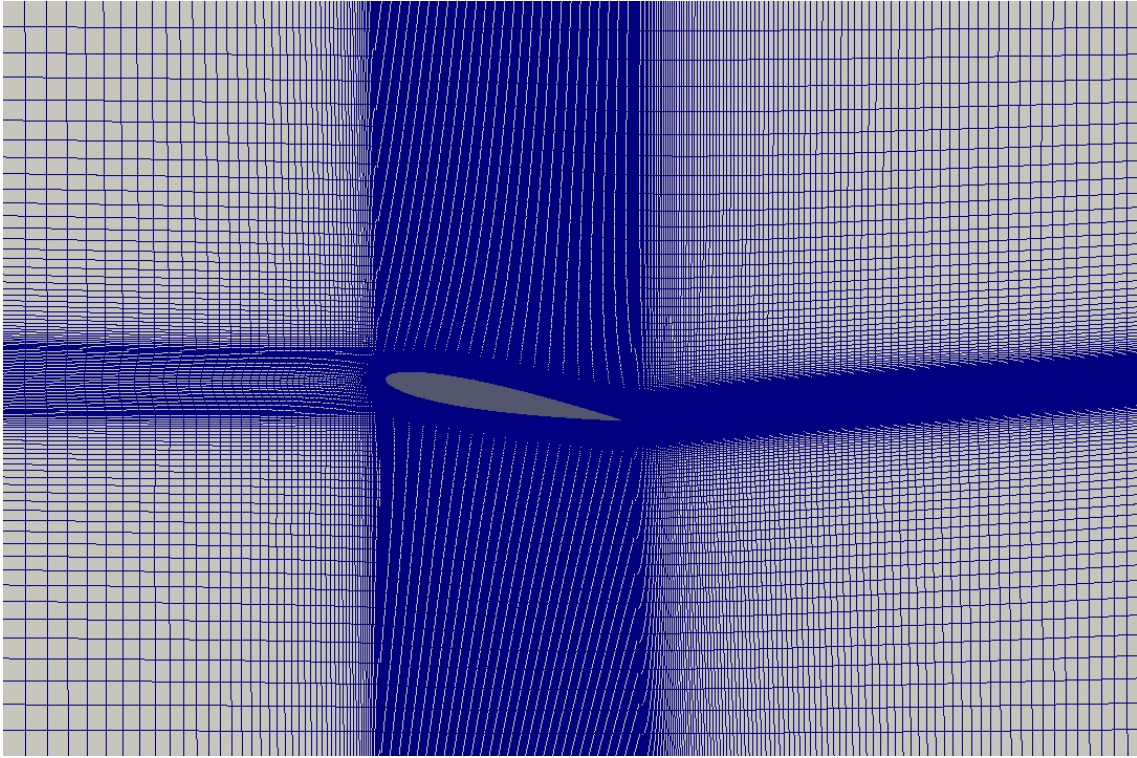


Figure 7: 10° rotation of the foil in Openfoam

In figure 7 we see that the foil has been rotated 10° . This rotation makes only the cells around the foil move whereas the cells on each end of the domain are not moving. On figure 8 the vortices are propagating downwards instead of propagating horizontally behind the foil. The reason of this behaviour could be due to the cells that are not moving everywhere correspondingly to the rotation of the foil.

8.3.1 Velocity plot in Paraview

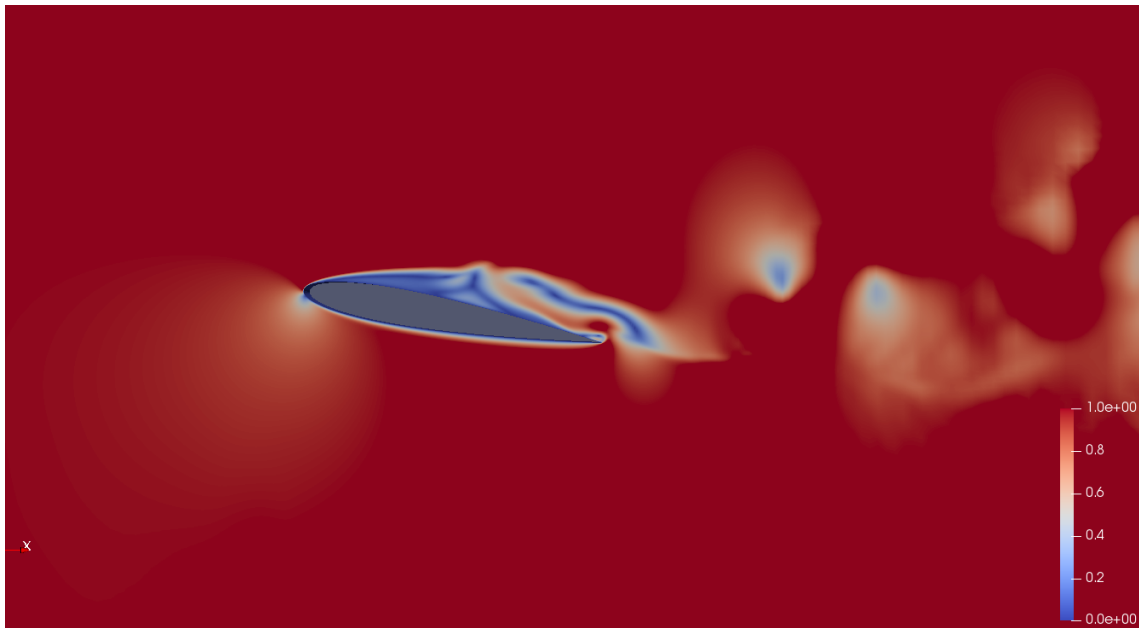


Figure 8: Velocity plot for $Re = 5000$ and $AOA = 10^\circ$

Figure 8 show a screenshot of the velocity. We see that the wake is propagating downwards and the flow seems to behave as if it was turbulent. If we compare to the pictures from Razavi et al. [17] the flow should be very streamlined.

8.3.2 Comparison of drag and lift coefficient

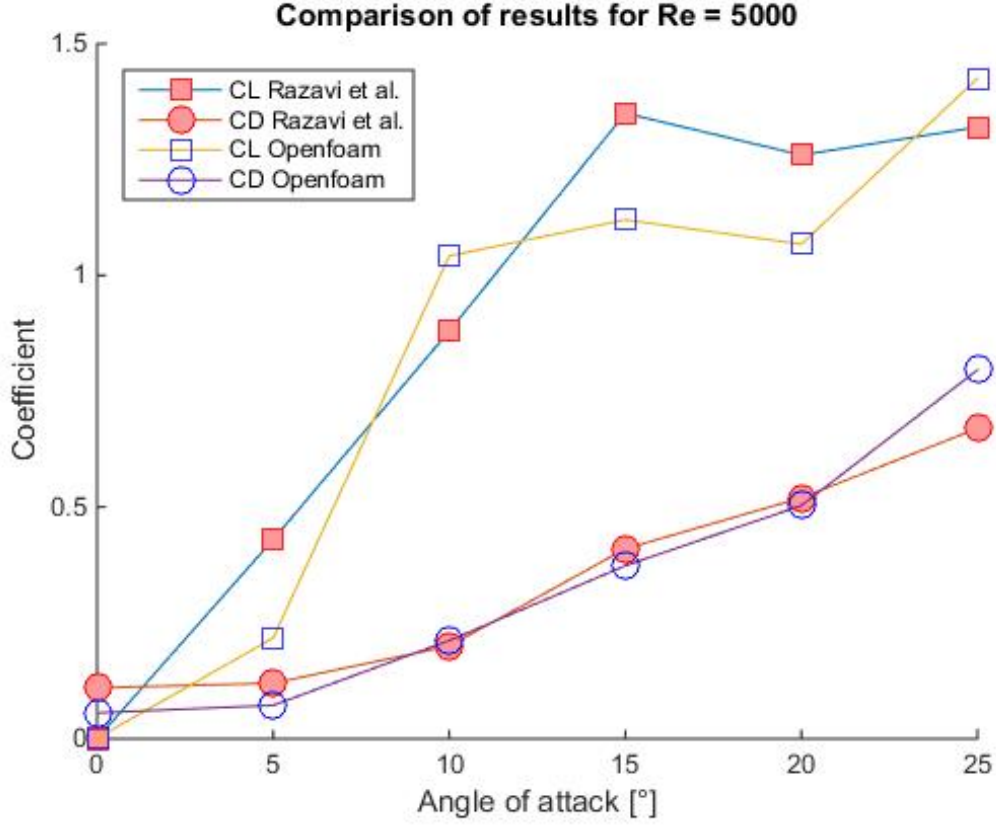


Figure 9: Final drag and lift coefficient compared with Razavi et al. [17]

The drag and lift coefficient in figure 9 are calculated as follow.

$$C_D = \frac{F_D}{\frac{1}{2}\rho U^2 A} \quad (7)$$

$$C_L = \frac{F_L}{\frac{1}{2}\rho U^2 A} \quad (8)$$

Where F_D and F_L are respectively the drag and lift force exerting on the foil, ρ is the density of the water, U the velocity magnitude and A the surface of the foil taken here as the chord-length times the width. The coefficients are obtained directly with a function in the Openfoam code. In figure 9 it can be seen that the values of the drag coefficient correspond quite well for most of the angles of attack whereas the lift coefficients are quite different. The highest difference is for $AOA = 5^\circ$ where the lift coefficient is half of the reference whereas it is quite close for $AOA = 25^\circ$. For a simple shape

of foil the value of the lift can be approximated with $C_L = 2\pi\alpha$ (Faltinsen [8]) which for 5° gives $C_L = 0.55$, more than twice the results obtained with Openfoam. The results from this stretchable grid are clearly not satisfying and a new strategy will be used in the next section.

8.3.3 Pressure coefficient plot

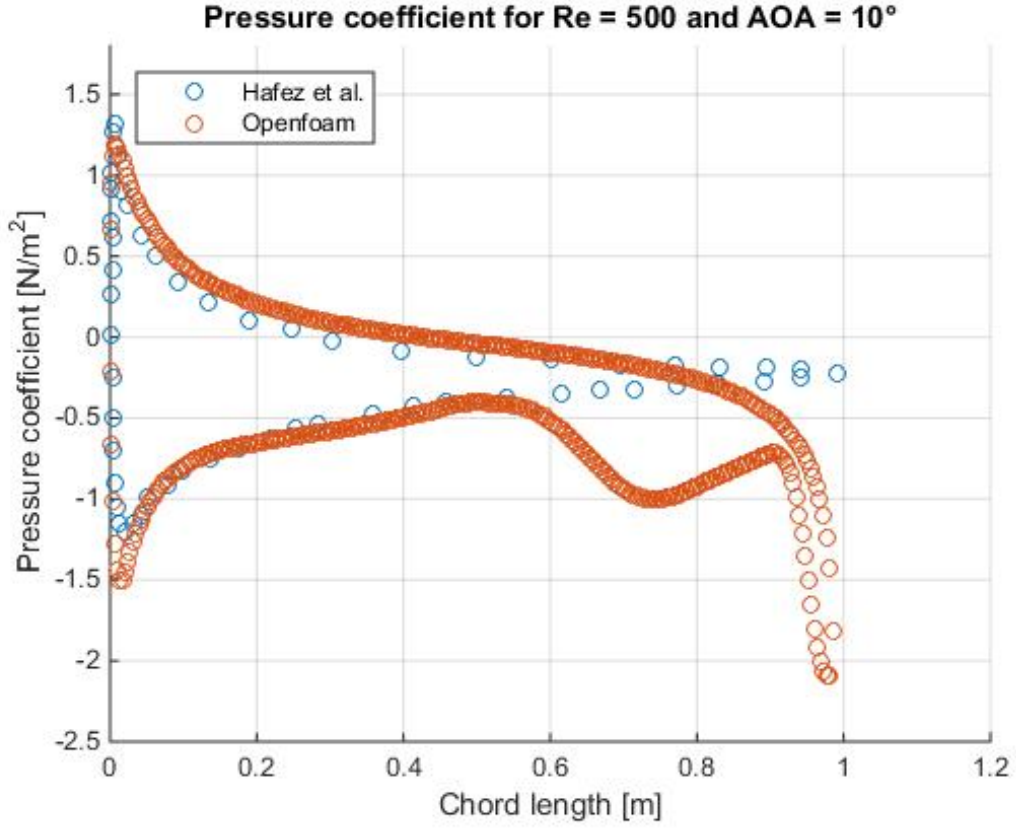


Figure 10: Pressure coefficient compared with Hafez et al. Results taken from Razavi et al. [17]

The pressure coefficient is calculated as follow.

$$C_P = \frac{P - P_\infty}{0.5\rho_\infty U_\infty^2} \quad (9)$$

Where P_∞ is the pressure far away in the flow, ρ_∞ is the density of the flow here equal to 1 and U_∞ is the velocity far away from the foil equal to 1. P is equal to the pressure on the foil. Since the pressure in Openfoam is given as the absolute pressure, equation 9 becomes

$$C_P = 2 * P_{abs} \quad (10)$$

Figure 10 shows the pressure obtained in Openfoam compared to Hafez et al. (Values taken from Razavi et al. [17]). There is clearly something wrong happening at the trailing edge. The C_p from Openfoam is higher on the suction side and lower on the pressure side but agrees quite well between 0.08 m to 0.5 m of the chord length. The difference at the leading edge could be due to too few cells. Furthermore, bigger domain sizes should also be tested to see the effect on the convergence of the C_p . But since the results at the trailing edge seem to be completely wrong this strategy of stretchable grid will not be studied more in depth.

- Flow features for simulations at $Re = 500$ and $AOA = 10^\circ$

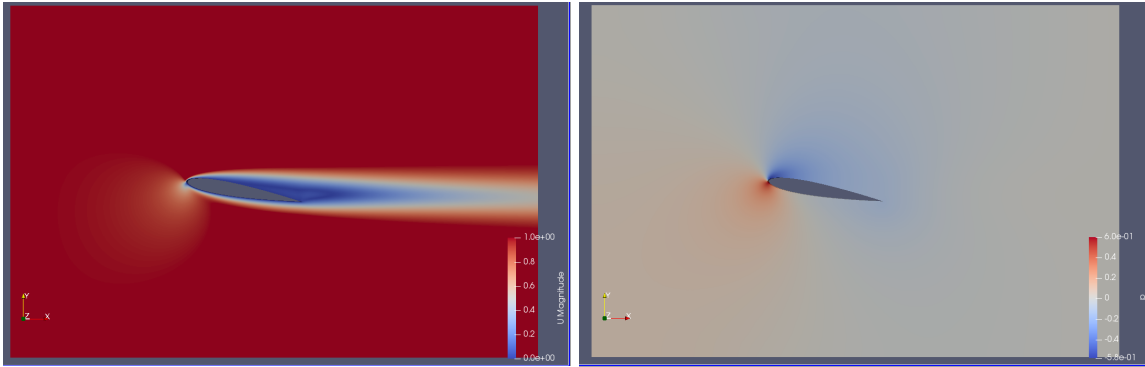


Figure 11: U magnitude for minimum lift [ms^{-1}] Figure 12: Pressure at minimum lift [m^2s^{-2}]

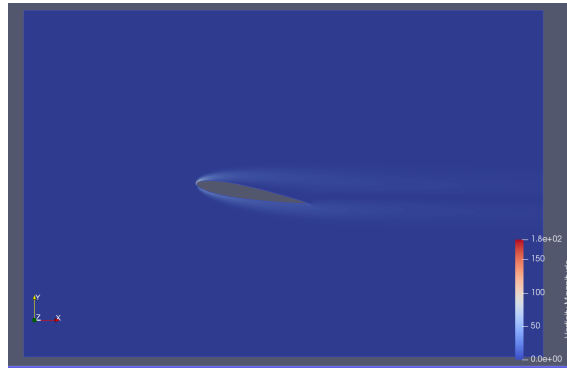


Figure 13: Vorticity at minimum lift [s^{-1}]

Figures 11, 12 and 13 show a screenshot of the simulation at $Re = 500$ and $AOA = 10^\circ$ at steady state. The flow is laminar and there is no vortex shedding. From the pressure plot it is difficult to describe what happens at the trailing edge but from the velocity there is some variations that could explain the singularity seen in figure 10.

8.3.4 Velocity at 20% and 80 % of chord length

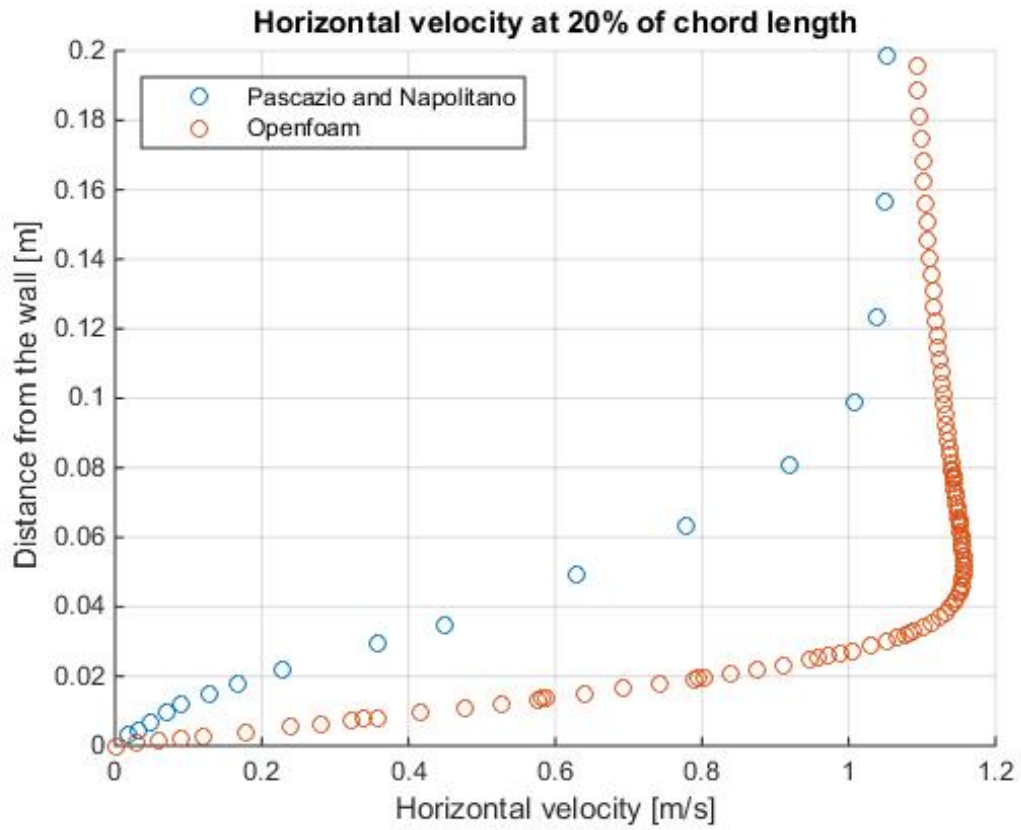


Figure 14: Comparison for $Re = 2000$ and $AOA = 0^\circ$ with Pascazio and Napolitano, results taken from Razavi et al. [17]

On figure 14 it can be seen that the results from Openfoam do not agree with the literature. The velocity from Openfoam is higher than the results from the literature.

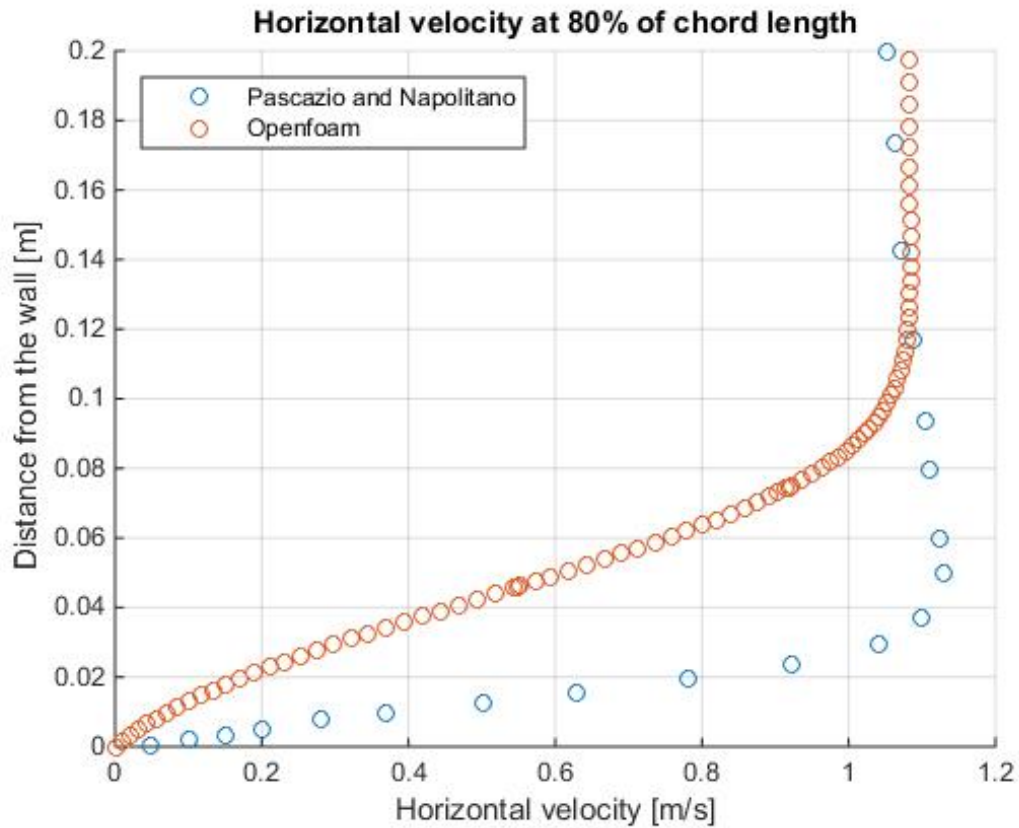


Figure 15: Comparison for $Re = 2000$ and $AOA = 0^\circ$ with Pascazio and Napolitano, results taken from Razavi et al. [17]

Similarly, as in figure 14 the results from Openfoam do not agree with the literature in figure 15. Figure 14 and 15 confirm that the stretchable grid is not a suited strategy for simulations of a static foil. This excludes also to make studies on a flapping foil with a stretchable grid. The next strategy will explore the overset grid strategy in Openfoam.

- Flow features for $Re = 2000$ and $AOA = 0^\circ$

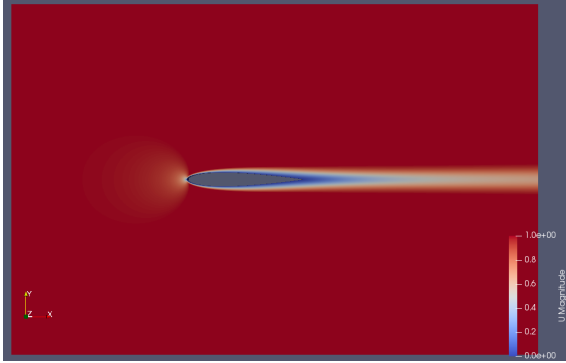


Figure 16: U magnitude for minimum lift $m s^{-1}$

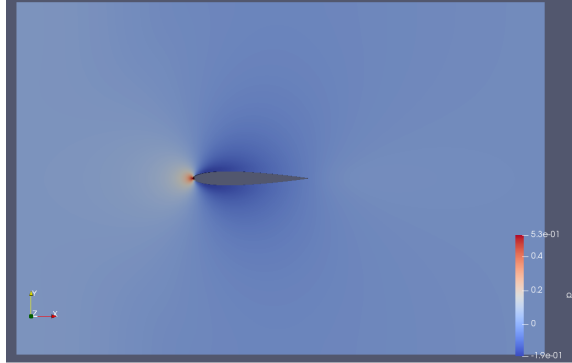


Figure 17: Pressure at minimum lift $[m^2 s^{-2}]$

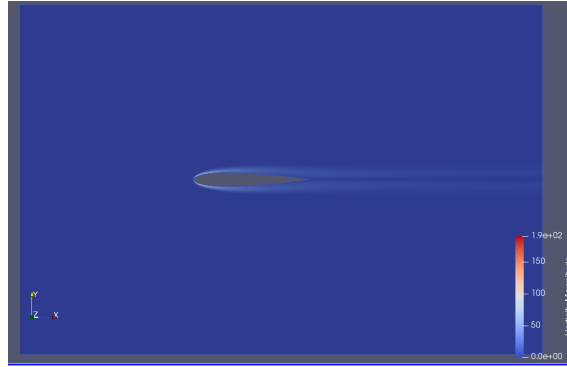


Figure 18: Vorticity at minimum lift $[s^{-1}]$

Figure 16, 17 and 18 show a screenshot of the simulation at $Re = 2000$ and $AOA = 0^\circ$ at steady state. The flow is laminar and there is no vortex shedding.

8.4 Overset grid

In the previous sections the simulations were compared against Razavi et al. [17] because this article compared many other sources from the literature. In the next sections the results are compared with Kurtulus [14] and with Bardazzi and Lugni (preliminary results, personal communications). Claudio Lugni was co-supervisor for this thesis and it was easier to discuss results in this way.

8.4.1 Assumptions in Openfoam

In this section the solver `overPimpleDyMFoam` is used for the simulations of a NACA0012 foil in a laminar flow ($Re = 1000$). The `overPimpleDyMFoam` solver is used for transient cases and suited for

incompressible and turbulent flow for moving mesh [1]. PimpleFoam is a combination of SIMPLE and PISO algorithms. SIMPLE stands for Semi-Implicit Method for Pressure linked equations. The turbulence model can be turned off and changed to laminar model. The characteristics of the overPimpleDyMFoam model correspond well to the flow characteristics this section will study.

Table 3: Boundary conditions

BC	Inlet	Outlet	Foil	Top and bottom	Front and back	Overset patch
P	Zero gradient	Fixed value = uniform 0	Zero gradient	Zero gradient	Empty	Overset uniform 0
U	Uniform value table	Zero gradient	Uniform(0,0,0)	Zero gradient	Empty	Overset uniform 0

The boundary conditions have been summarized in table 2. The BC for front and back planes are set to empty since this is a 2D simulation. The velocity on the foil is defined as Uniform(0,0,0) which means no slip. The pressure on the foil is defined as zero gradient because there is no pressure variation inside the foil. At the inlet the velocity is set to uniform value table to make the velocity increase progressively to (1,0,0) to avoid too big CFL numbers. The pressure at the inlet is set to zero gradient because the pressure is constant. At the outlet the velocity is set to zero gradient because there is no change in velocity. The pressure is zero at the outlet. On the top and bottom of the domain the velocity and pressure are constant in order not to disturb the flow. This is therefore defined in Openfoam as zero gradient.

8.4.2 Strategy

The overset grid is composed of three different grids. A bodyfitted grid for the foil (Hui-li Xu, personal communication), a background grid and a small rectangle grid that will make the transition between the bodyfitted grid and the background-grid smooth. The strategy used in the beginning is to make a c-grid for the foil that is big enough to capture the boundary layer. The bodyfitted grid is merged with the small rectangle and are rotated together in the dynamic mesh in Openfoam. The size of the bodyfitted grid is set depending on the boundary layer thickness. The boundary layer thickness has been calculated as follow using the flatplate assumption from Blasius [4].

$$\delta = \frac{4.91x}{\sqrt{Re_x}} \quad (11)$$

In our case for $Re = 5000$ and $x = 1$, δ is about 0.1. Notice that this grid was originally thought to be used for $Re = 5000$ but was also used for $Re = 1000$.

8.5 Boundary fitted grid

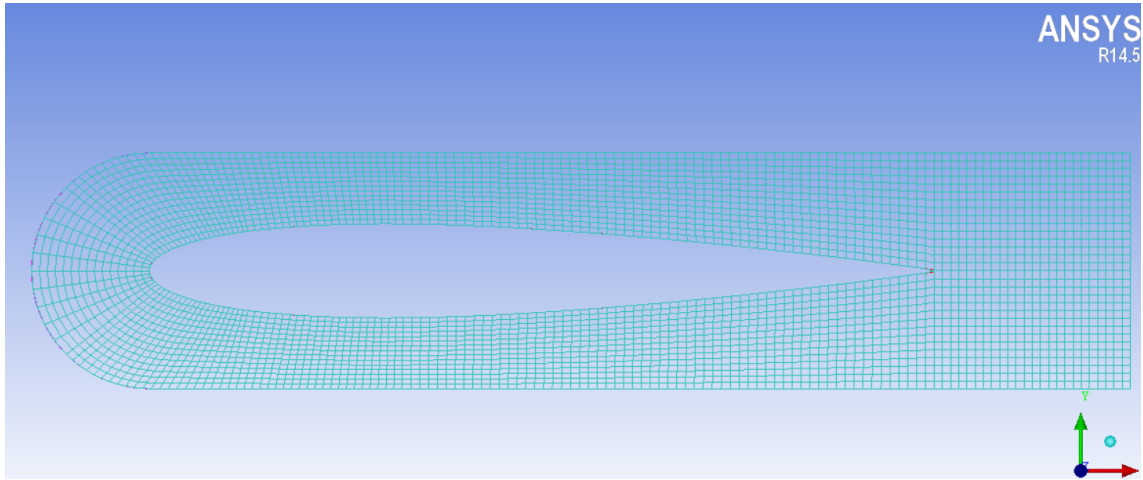


Figure 19: Body-fitted Grid

Figure 19 shows the bodyfitted grid around the foil. The challenge for the grid around the foil is to make the cells uniform everywhere. This is quite difficult and the cells at the leading edge are therefore larger.

8.5.1 Entire grid

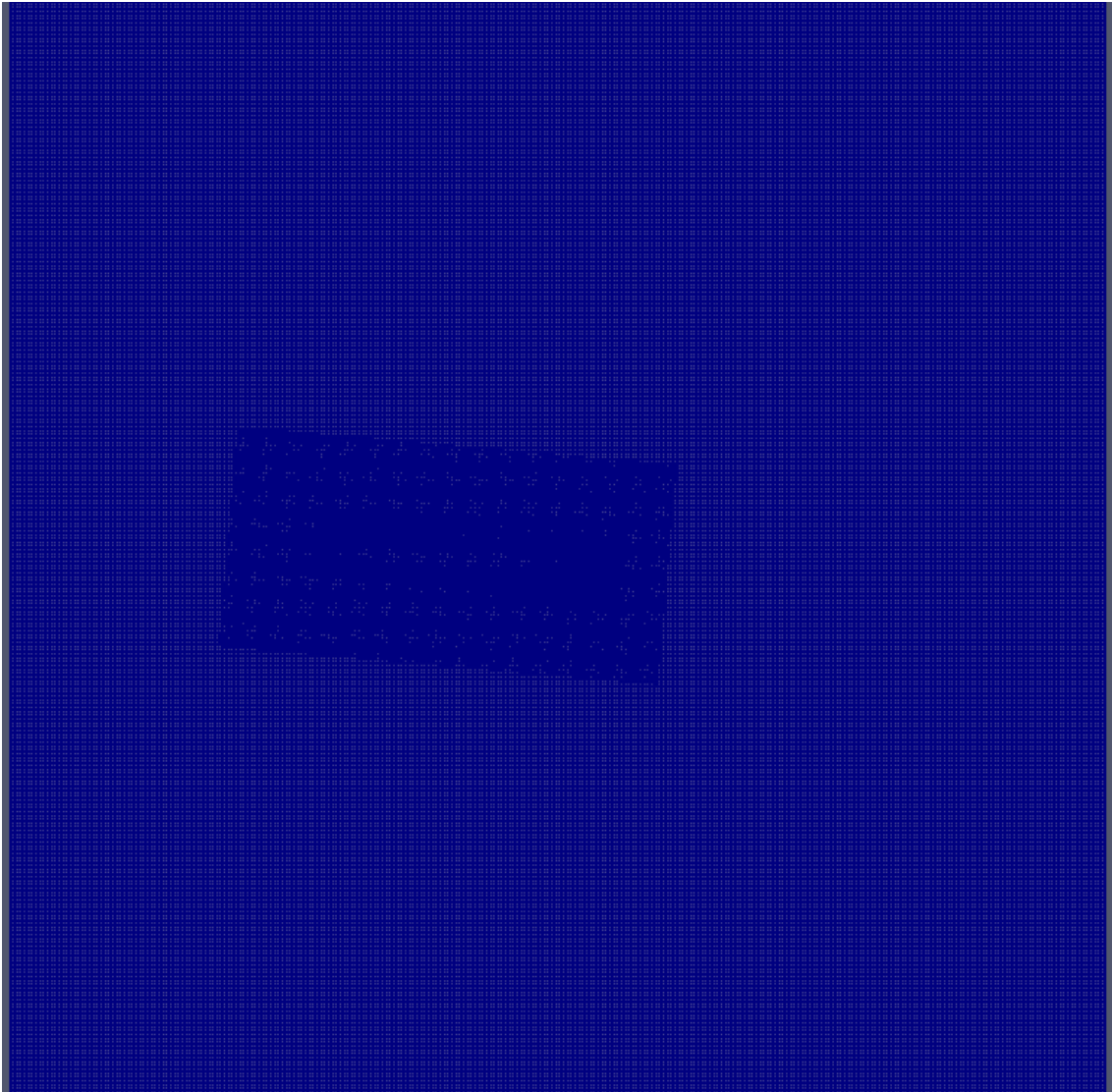


Figure 20: Entire domain seen in Paraview

Figure 20 shows the entire domain seen in Paraview. The boundaryfitted grid, the refinement grid and the background domain can be seen.

8.5.2 Refinement zone

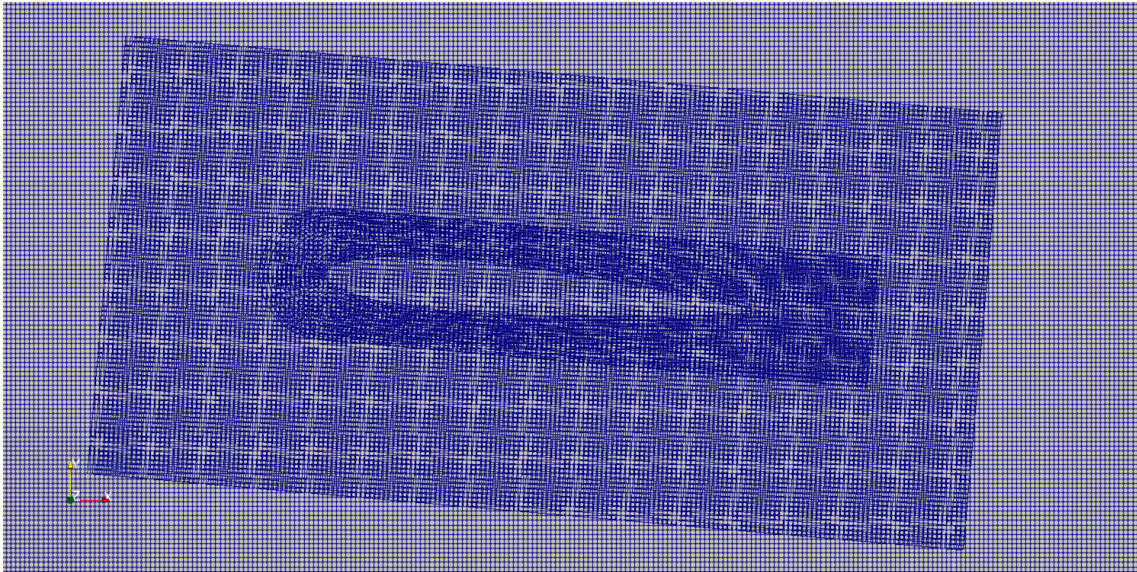


Figure 21: Refinement zone

Figure 21 shows a zoom of the refinement zone and the bodyfitted grid.

8.5.3 Drag and lift coefficient

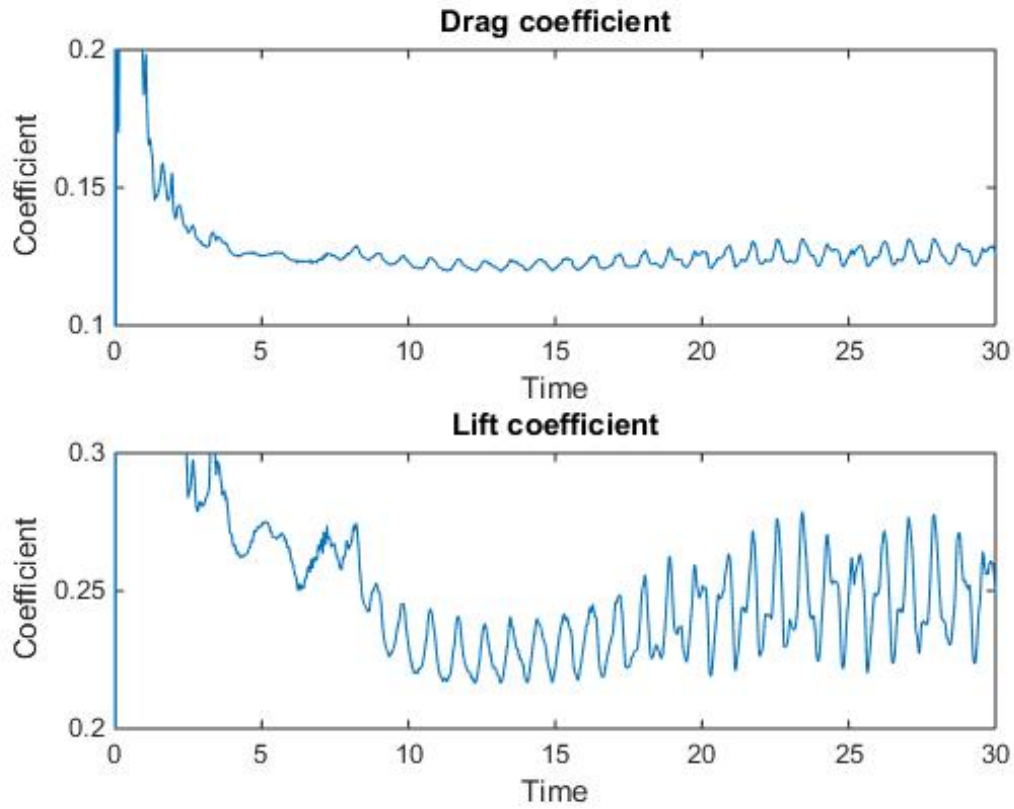


Figure 22: Drag and lift coefficients versus time for $Re = 5000$ and $AOA = 5^\circ$

A time series for drag and lift coefficients can be seen in figure 22. The simulation was run for 30 seconds and it seems that the flow didn't reach a steady state. The C_D and C_L don't oscillate in a regular manner.

8.5.4 Comparison of drag and lift coefficients

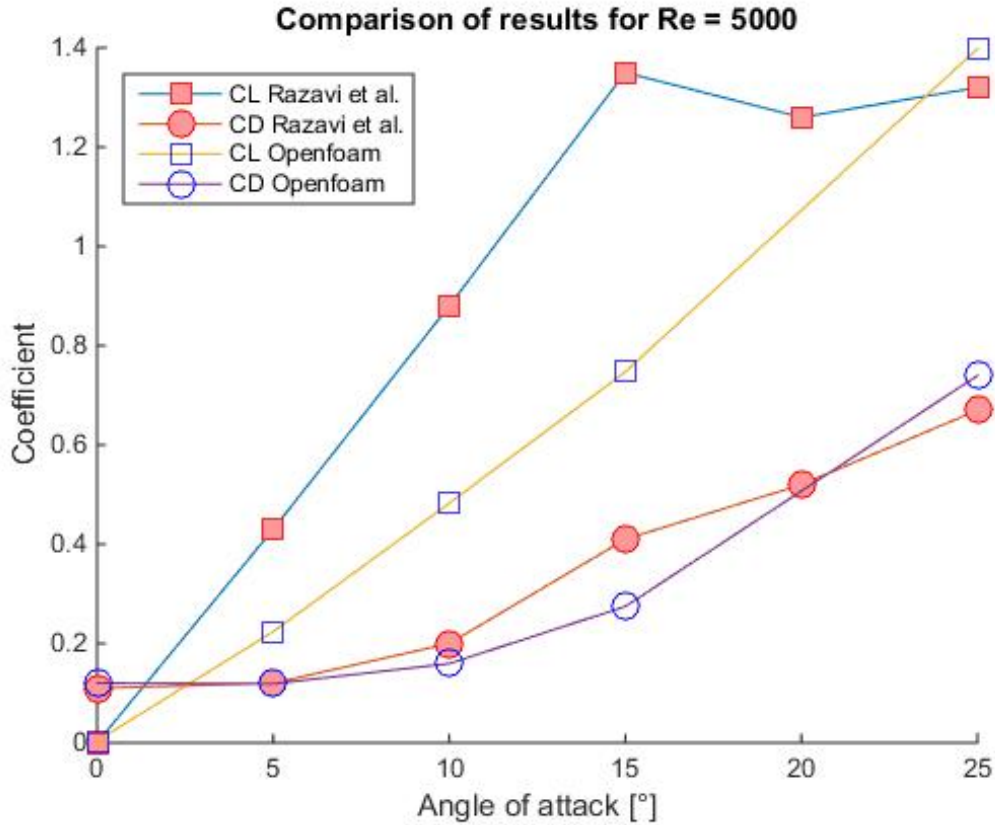


Figure 23: Final drag and lift coefficient compared with Razavi et al. [17]

Notice that there are no results for $AOA = 20^\circ$. The simulation ran less than one second and stopped. Further down in this thesis the ramp function has been introduced to avoid an explosion of the solution at the beginning of the simulation. The ramp function allows to increase the inlet velocity gradually from zero to $1 \text{ m} \cdot \text{s}^{-1}$. The reason why the simulation didn't run at 20° could maybe have been avoided using this function. Since this was discovered later in the thesis and since the results in this section were not satisfying, the ramp function was not tested here. On figure 23 it can be seen that the values of the drag coefficient are quite similar to the reference paper whereas the values of the lift coefficient are still very different. For 25° the value is almost the same but for the other there is still a big difference. The difference between the results with overset strategy and the moving point strategy is that the values are linear until 15° as for the reference paper. The drag and lift coefficients were calculated on the last 5 seconds due to the unstable period. The next step would have been to plot the pressure coefficient around the foil and compare with the literature but the threshold function emphasized a discontinuity between the bodyfitted fitted grid and the

refinement grid. This can be seen in figure 27 and 28.

8.5.5 Discontinuity between grids

After more in depth investigation about the flow in Paraview it was discovered a discontinuity in the flow between the bodyfitted grid and the refinement grid. Experiments have later shown that this discontinuity disappeared when using only two grids instead of three. The following sections show pictures of the grid and the discontinuity.

- Results with overset using three grids

Table 4: Drag and lift coefficients compared with Kurtulus [14]

Case	Cd	Cl
Results from Kurtulus [14]	0.69	0.28
100 cells	0.8542	0.3770
232 cells	0.7910	0.3364

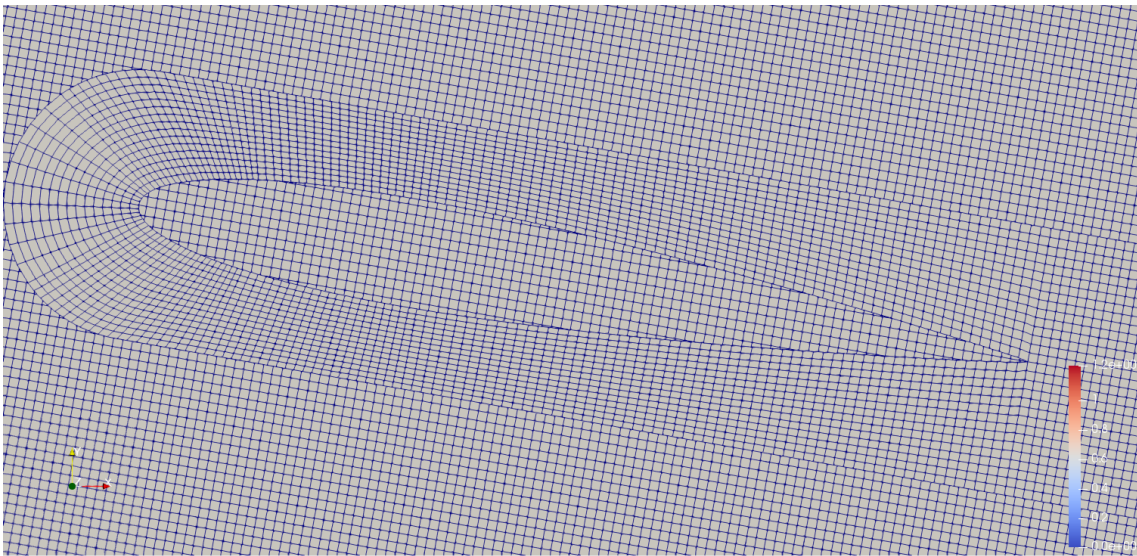


Figure 24: View of the body fitted grid and refinement grid

Figure 24 shows the body fitted and refinement grid in Paraview. The body fitted grid cell size and the refinement grid cell size are of the same order.

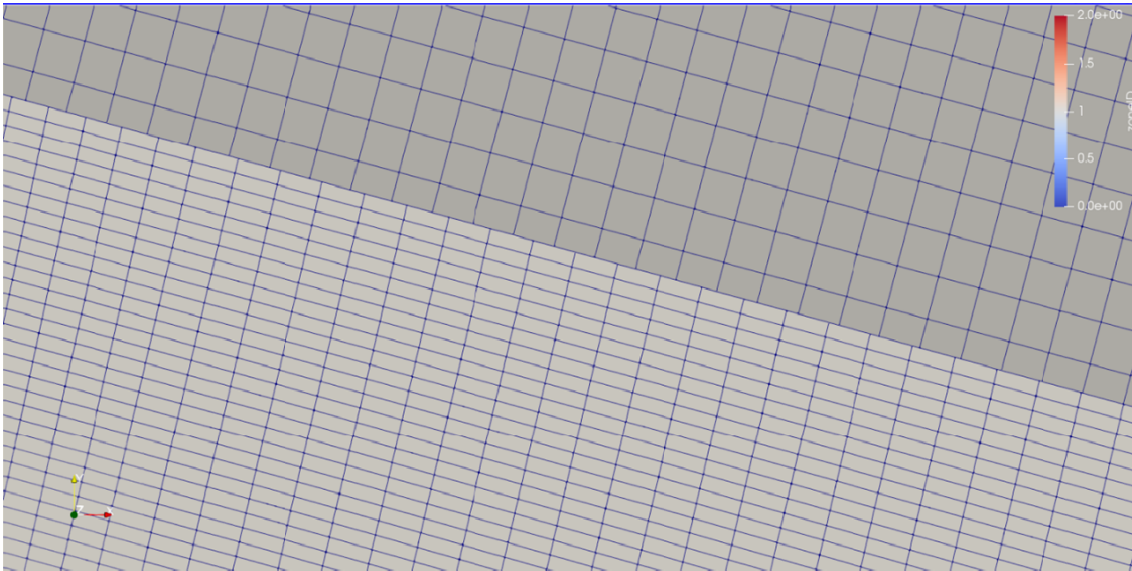


Figure 25: Boundary region between bodyfitted grid and refinement grid

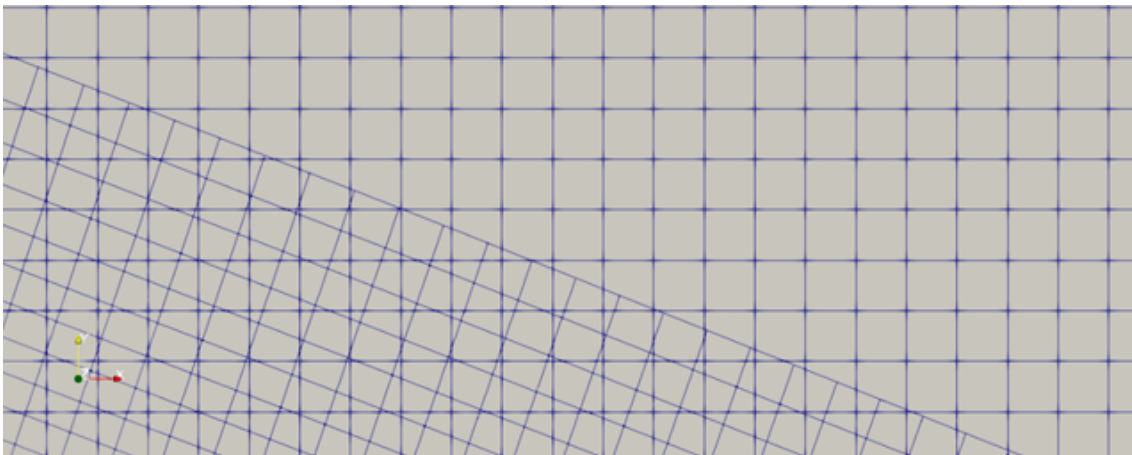


Figure 26: Boundary region between refinement grid and background grid

Figure 25 and 26 show the cells size at the boundary region for each grid. The cells for the bodyfitted grid are more rectangular than for the refinement grid but the order of size is similar.

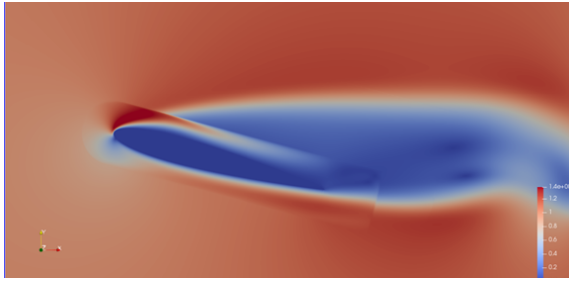


Figure 27: Period of drag function of domain size



Figure 28: Discontinuity in the vorticity

Figure 27 and 28 show the discontinuity that appears between the body fitted grid and refinement grid. In Paraview this discontinuity is not possible to observe at the first look, some parameters have to be adjusted to be able to see it. This was done using the threshold function in Paraview that separates each grid. The grids are then seen separately. We can see that the parallel run using three different grids causes issues in the supercomputer Vilje and it seems that the reconstruction of the results is not properly done. In the next section it will be shown that using two grids with hierarchical decomposing works and gives better results and avoids the discontinuity. The next section will also show the final convergence study with two grid systems.

8.6 Convergence study

In this section the convergence study for a simulation with two grids is presented. Using two grids means that there are more cells in the domain. The bodyfitted grid was also improved by Hui-li Xu (personal communication).

8.6.1 Improved bodyfitted grid

Hui-li Xu made this body fitted grid in ICEM (personal communication). The contours of the grid follow much better the shape of the foil and make the cells all around the body almost perfectly perpendicular to the body surface. Still the size of the cells at the front area is more elongated. Figure 29 shows the body fitted grid.

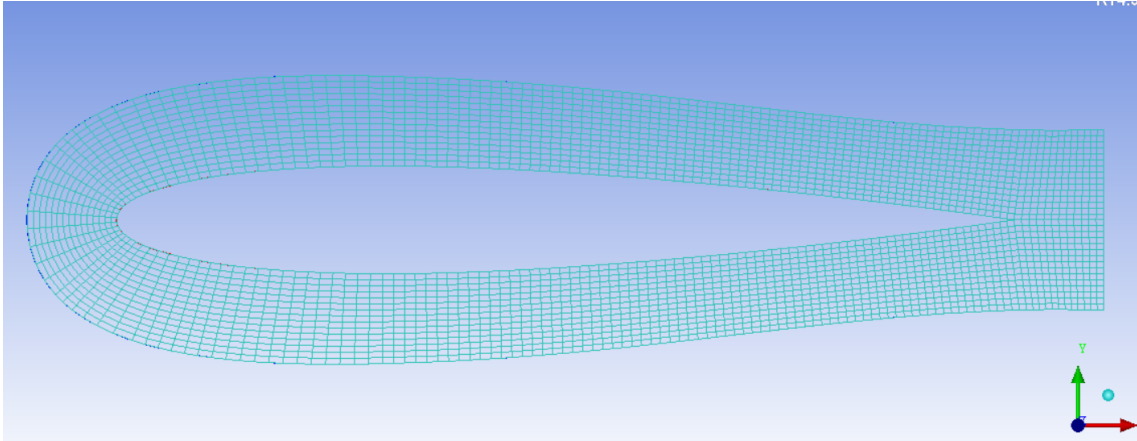


Figure 29: Improved bodyfitted grid

8.6.2 Domain convergence study

Table 5: Parameters of the different cases and results for C_D and C_L

Case	Domain size	Number of cells	Number of cells along the foil	C_d	C_l
DM	$L = -5c+6c, H = \pm 6c$	2658886	208	0.2877	0.7055
DB	$L = -5c+6c, H = \pm 6c$	5324806	208	0.2874	0.7050
DS	$L = -5c+6c, H = \pm 6c$	1311106	208	0.2885	0.7058
GC	$L = -5c+6c, H = \pm 6c$	1183396	162	0.3003	0.7254
GF	$L = -5c+6c, H = \pm 6c$	5420476	293	0.2821	0.6921
Kurtulus	-	-	-	0.28	0.69

In table 5 the main parameters of the cases tested in the convergence study can be seen. The drag and lift coefficients are compared against results from Kurtulus [14].

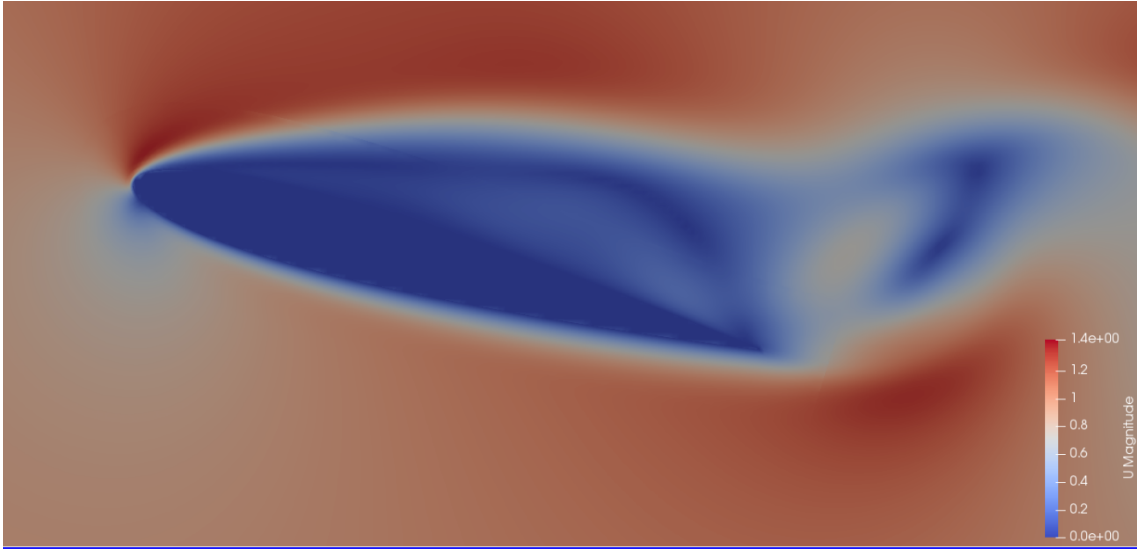


Figure 30: Threshold

Figure 30 shows the flow around the foil using the threshold function in Paraview. The flow is almost perfectly continuous. A tiny mark on the top at the beginning of the foil can be seen. This could be avoided by adjusting the size of the cells at the boundary of the body fitted grid.

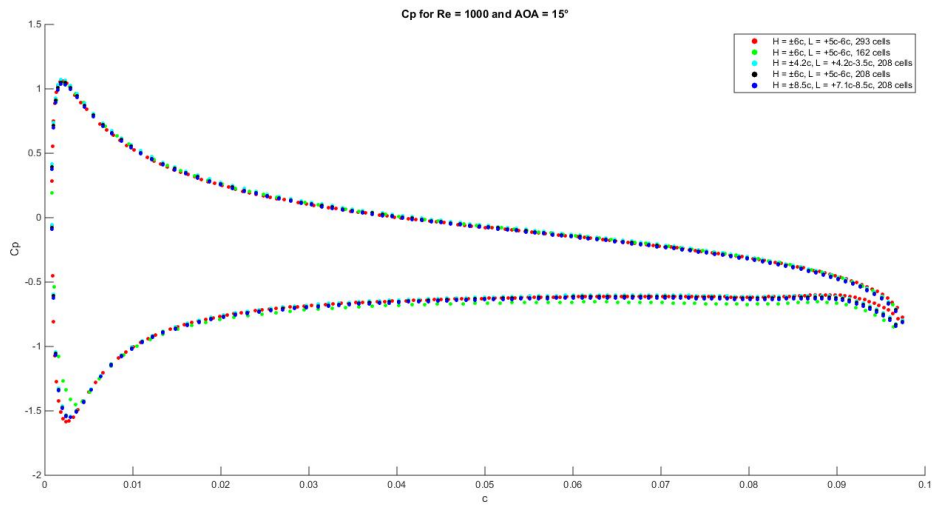


Figure 31: Cp for all the cases

The pressure coefficient C_P can be seen in figure 31 for all the cases. All the cases are quite similar except at the leading and trailing edge where the difference is the most significant. The green

curve corresponding to the coarsest cell size is clearly different from the other cases at the trailing and leading edge.

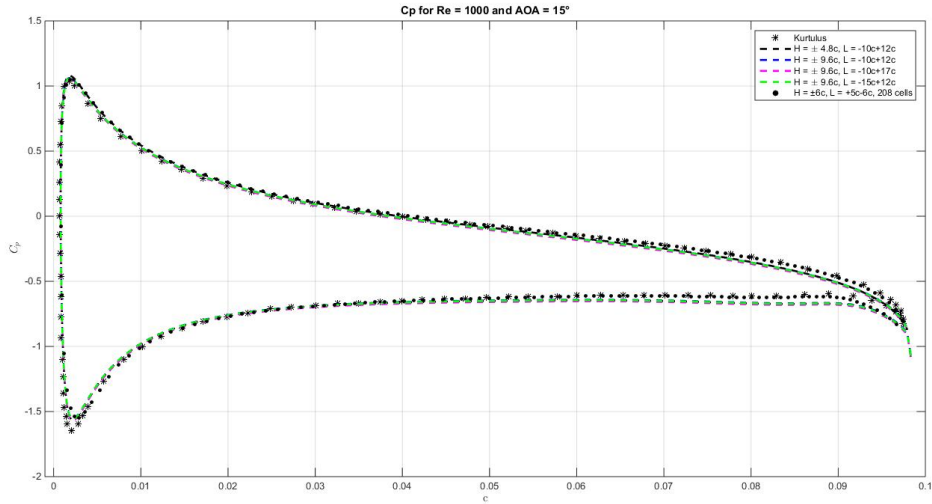


Figure 32: C_p for medium cell size against Kurtulus

Figure 32 shows the medium domain size. At the trailing edge the curve is located between the results of Kurtulus [14] and the results of Bardazzi and Lugni (preliminary results, personal communication). At the leading edge the curve follows the results from Bardazzi and Lugni.

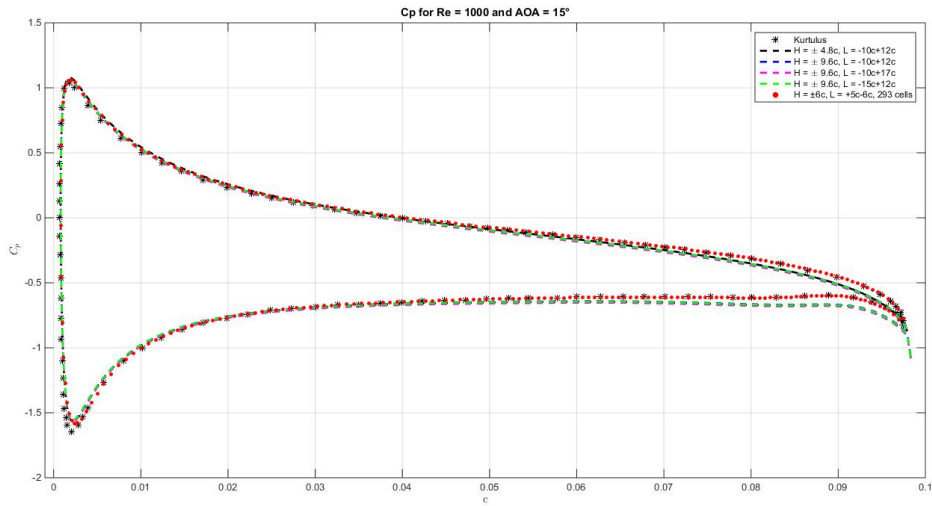


Figure 33: C_p for finest cell size against Kurtulus

Figure 33 shows the curve in red from the finest cell size against Kurtulus [14] and Bardazzi and Lugni (preliminary results, personal communication). The Curve follows almost exactly Kurtulus except there is a tiny difference at the leading edge and at the very end of the trailing edge.

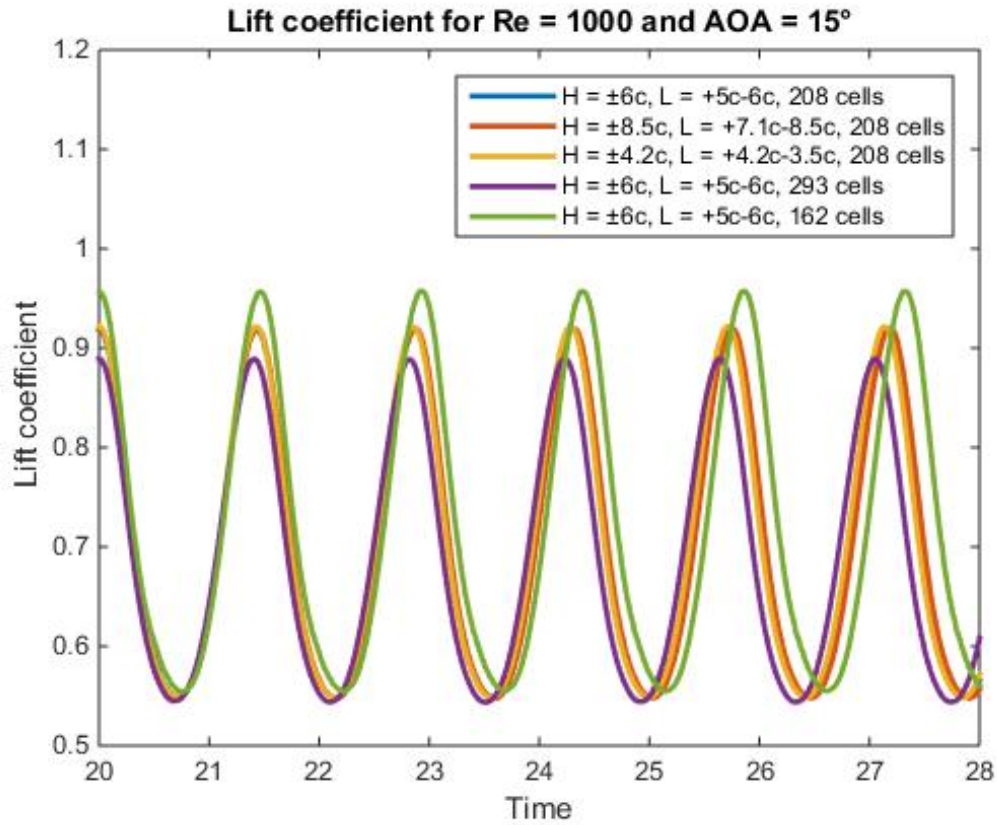


Figure 34: Lift coefficient

The lift coefficients for all the cases have been plotted in figure 34. The change in domain size does not affect significantly the lift coefficient whereas change in number of cells along the foil has more effect. The amplitude decreases with increasing the number of cells.

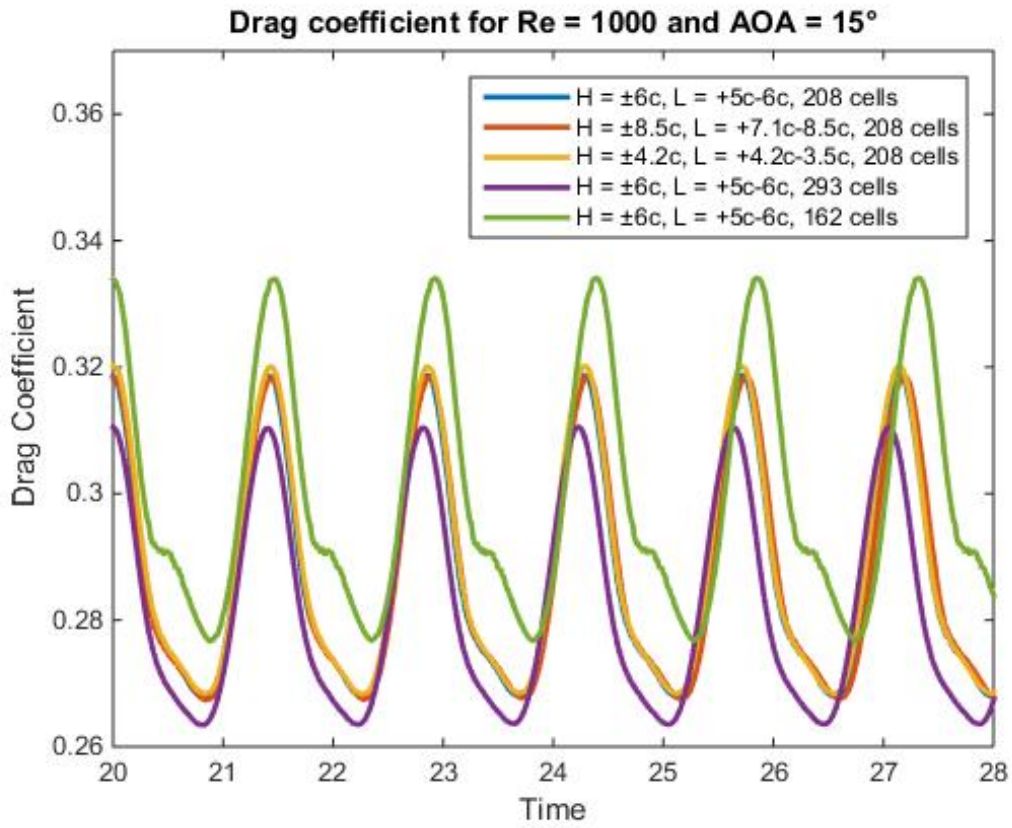


Figure 35: Drag coefficient

Similarly than in figure 34 the drag coefficients for all the cases have been plotted in figure 35. The change in domain size does not affect significantly the drag coefficient whereas change in number of cells along the foil has more effect. The amplitude decreases with increasing the number of cells.

8.6.3 Cell size convergence study

Table 6: Parameters and results of the cell size convergence study

Parameter/case	Case 1C	Case 2C	Case 3C
Cell number along the foil	162	208	293
Multiplication factor	-	1.2839	1.4187
Mean drag (figure 36)	0.2998	0.2877	0.2820
Change in % for mean drag	-	-4.0360	-1.9812
Mean lift (figure 37)	0.7222	0.7066	0.6935
Change in % for mean lift	-	-2.1601	-1.8539
RMS drag (figure 38)	0.3004	0.2882	0.2824
Change in % for RMS drag	-	-4.0612	-2.0125
RMS lift (figure 39)	0.7361	0.7186	0.7042
Change in % for RMS lift	-	-2.3774	-2.0039
Drag period (figure 40)	1.463	1.43	1.404
Change in % for drag period	-	-2.2556	-1.818
Lift period (figure 41)	1.463	1.43	1.412
Change in % for lift period	-	-2.2556	-1.2587

In table 6 the results from the cell size convergence study are summarized. The first case has 162 cells along the foil, case 2C has 208 cells and case 3C has 293 cells. The number of cells was increased by $\sqrt{2}$ and then the number was slightly adjusted in ICEM. The change from case 1C to case 2C and from case 2C to case 3C is also shown in table 6. The results in table 6 and the corresponding figures 36, 37, 38, 39, 40 and 41 show that the variation between case 2C and 3C (-1.2587 % to -2.0039 %) is much lower than between case 1C and 2C (-2.2556 % to -4.0612 %). Since the variation from case 2C to case 3C is lower than 2.0039 % it is assumed that case 2C gives satisfying results. Then if we consider the running time in Vilje, choosing case 2C is a good compromise since it gives reasonable results and the running time for 30 seconds of simulation is 3,4 hours. Which is much lower than case 3C with 37.5 hours of simulation time.

Table 7: Order of accuracy for the cell size convergence study

	OA mean cell size	OA maximum cell size
Mean drag	3.7	3.2
Mean lift	1.7	0.5
RMS drag	3.7	3.2
RMS lift	1.8	0.6
Drag period	1.9	3
Lift period	4.7	3

In table 7 the order of accuracy has been calculated for the same parameters than in table 6. The OA was calculated for the mean cell size and the biggest cell size in the domain. The mean cell size is calculated as the chord length of the foil divided by the number of cells along the foil. The maximum cell size was measured in ICEM. It was intended to include the OA for the smallest cell size but because of a small error in ICEM the smallest cell in case 1C was bigger than in case 2C so it would not have given good results. The corresponding values for each domain are summarized in table 8 below. The OA is comprised between 0.6 and 4.7 which is acceptable for Openfoam since the order of OA for Openfoam is 2. This confirms that the results are converging. The formula for the order of accuracy is taken from Collicchio et al. [9].

Table 8: Parameters used for the OA analysis

	1C	2C	3C
Mean cell size [m]	$\frac{1}{81}$	$\frac{1}{104}$	$\frac{1}{147}$
Maximum cell size [m]	0.03	0.02	0.013

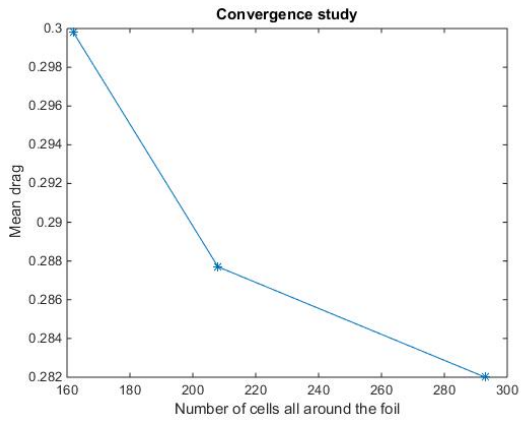


Figure 36: Mean drag function of number of cells along the foil

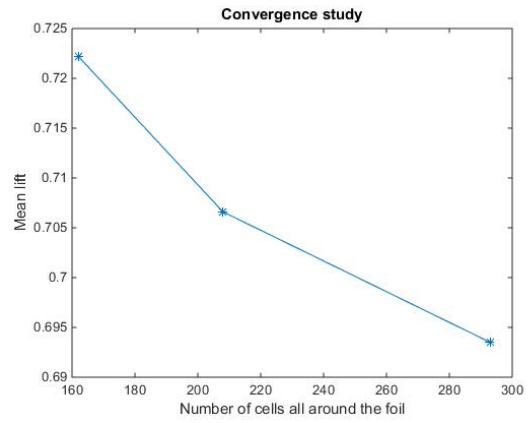


Figure 37: Mean lift function of number of cells along the foil

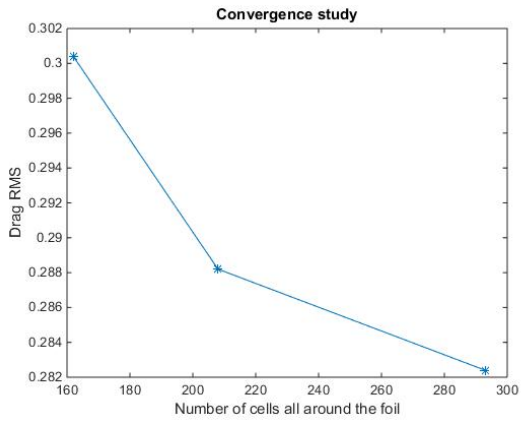


Figure 38: RMS of drag function of number of cells along the foil

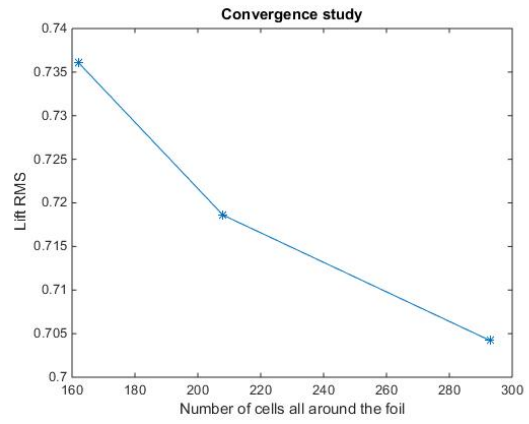


Figure 39: RMS of lift function of number of cells along the foil

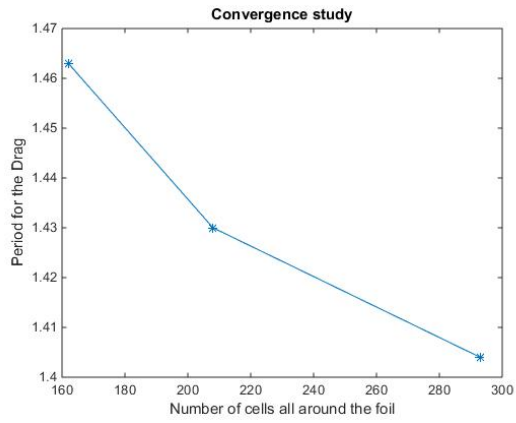


Figure 40: RMS of drag function of number of cells along the foil

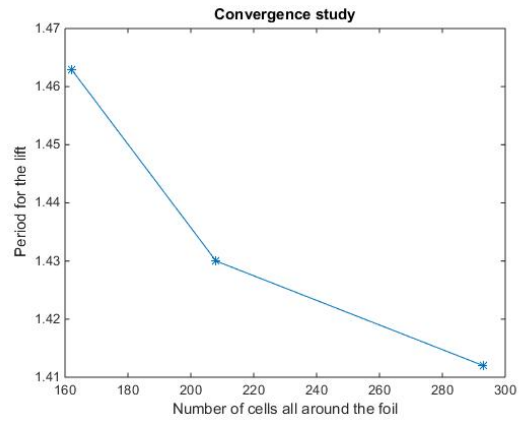


Figure 41: RMS of lift function of number of cells along the foil

8.6.4 Domain convergence study

Table 9: Parameters and results for the domain size convergence study

Parameter/case	Case 1D	Case 2D	Case 3D
Area [m^2]	64.68	132	265.2
Multiplication factor	-	~ 2	~ 2
Mean drag (figure 42)	0.2886	0.2877	0.2873
Change in % for mean drag	-	-0.3119	-0.1390
Relative error for mean drag [%]	0.4525	0.1392	-
Mean lift (figure 43)	0.7076	0.7066	0.7060
Change in % for mean lift	-	-0.1413	-0.0849
Relative error for mean lift %	0.2266	0.0850	-
RMS drag (figure 44)	0.2892	0.2882	0.2879
Change in % for RMS drag	-	-0.3458	-0.1041
Relative error for RMS drag %	0.4515	0.1042	-
RMS lift (figure 45)	0.7199	0.7186	0.7182
Change in % for RMS lift	-	-0.1806	-0.0557
Relative error for RMS lift %	0.23678	0.0557	-
Drag period (figure 46)	1.425	1.43	1.435
Change in % for drag period	-	0.3509	0.3497
Relative error for drag period %	0.6968	0.3484	-
Lift period (figure 47)	1.425	1.43	1.435
Change in % for lift period	-	0.3509	0.3497
Relative error for lift period %	0.6968	0.0.3484	-

In table 9 the results from the domain size convergence study are summarized. The first case has an area of $64.68 m^2$, case 2D $132 m^2$ and case 3D has $293 m^2$. Respectively the length and the height of the domain were increased with a factor $\sqrt{2}$ which means that the domain in case 2D is twice the one in case 1D and the domain in case 3D is twice the one in case 2D. The change from case 1D to case 2D and from case 2D to case 3D is also shown in table 9. The relative error for case 1D and 2D is also calculated with case 3D which is assumed to be the correct value. The relative error for case 2D is always much lower than for case 1D. The results in table 9 and the corresponding figures

42, 43, 44, 45, 46 and 47 show that the variation between case 2D and 3D (-0.0849% to 0.3497%) is much lower than between case 1D and 2D (-0.1413% to 0.3509%). Since the variation from case 2D to case 3D is lower than 0.3497 % it is assumed that case 2D gives satisfying results. Case 2D in this section is the same as case 2D in the previous section. Case 2D seems therefore to be a good compromise between running time in Vilje and accuracy of results and will be used for the final simulation of the thesis.

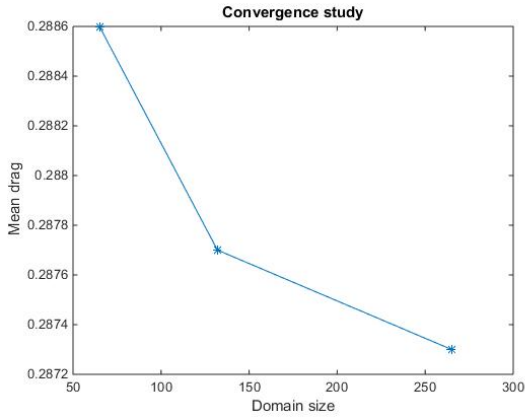


Figure 42: Mean drag function of domain size

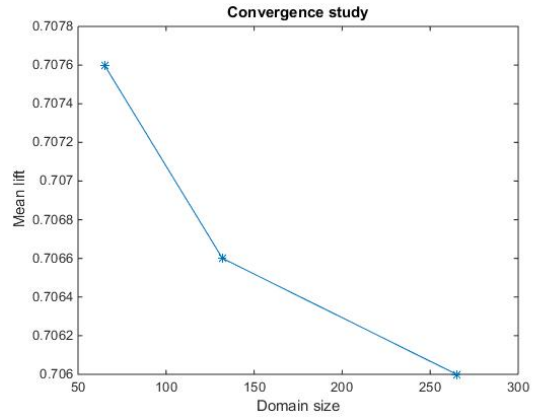


Figure 43: Mean lift function of domain size

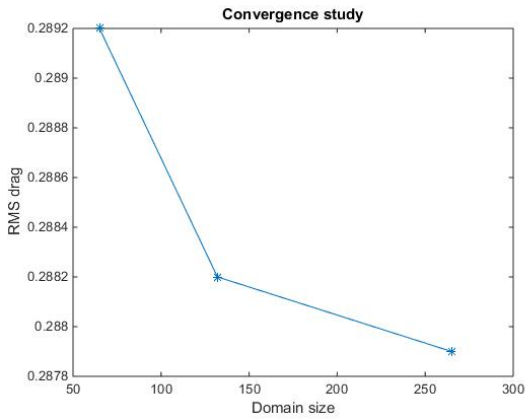


Figure 44: RMS of drag function of domain size

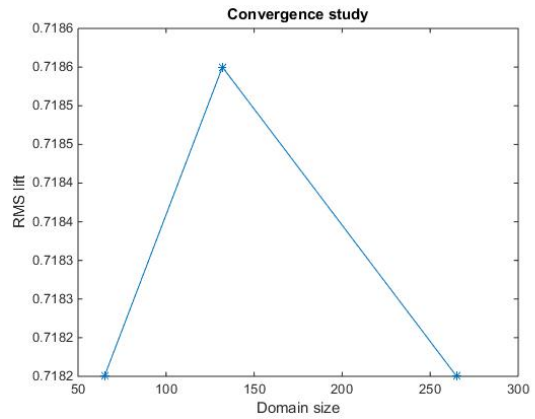


Figure 45: RMS of lift function of domain size

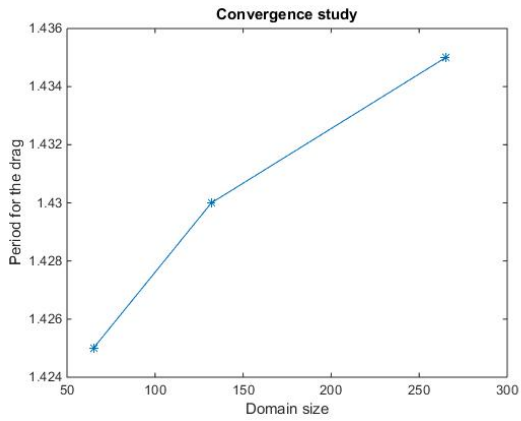


Figure 46: Period of drag function of domain size

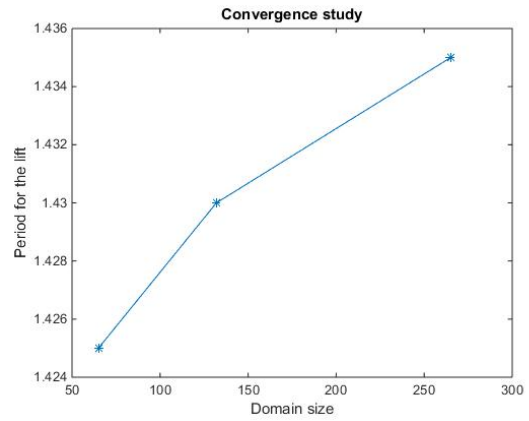


Figure 47: Period of lift function of domain size

The choice of the case to use for the moving foil is made as a compromise between running time and accuracy of results. Case 3C has significantly higher running time (about 20 hours) compared to 2C. Case 3D has also a much higher running time than case 2D. Case 2D and 2C being the same case, it will be suited for the motion simulations. Screenshots of the velocity, pressure and vorticity at different stages of the phase are shown on next page for case 2C.

8.6.5 Flow features

A screen shot from the velocity magnitude, the pressure and the vorticity can be seen for maximum lift, minimum lift and between maximum and minimum lift. The three stages represent a half period of oscillation of the lift produced by the foil.

- At maximum lift

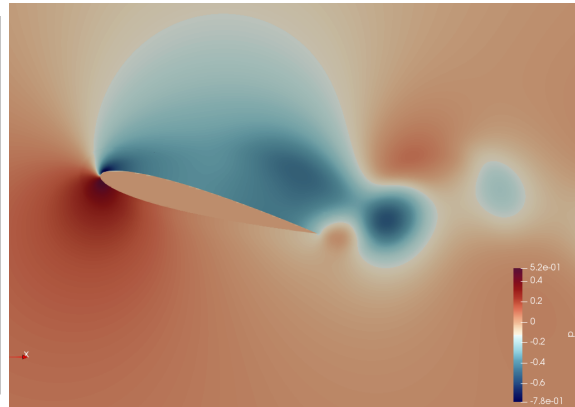
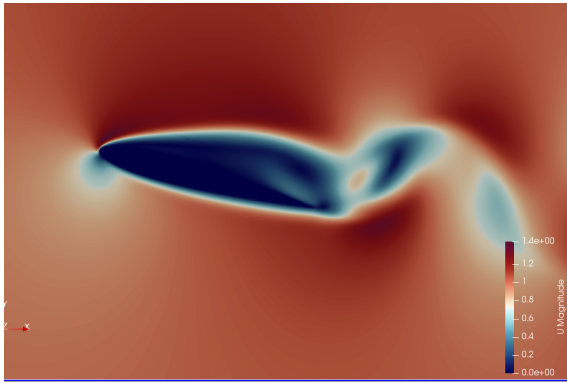


Figure 48: U magnitude for maximum lift [ms^{-1}]

Figure 49: Pressure at maximum lift [m^2s^{-2}]

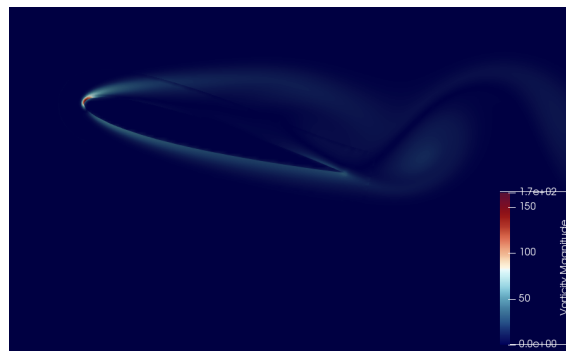


Figure 50: Vorticity at maximum lift [s^{-1}]

In figure 48, 49 and 50 the flow features for maximum lift can be seen. A vortex shedding is starting to appear at the trailing edge. The velocity and the vorticity are lower on the pressure side of the foil.

- Between maximum and minimum lift

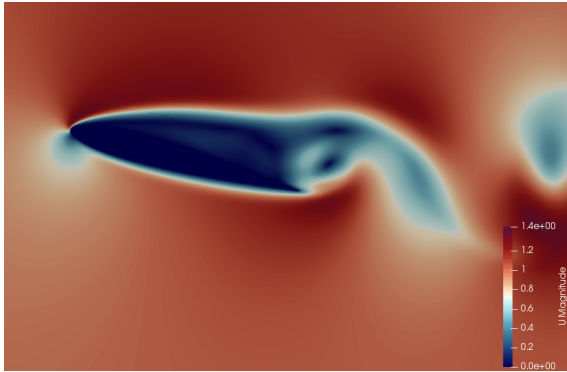


Figure 51: U magnitude between maximum and minimum lift [ms^{-1}]

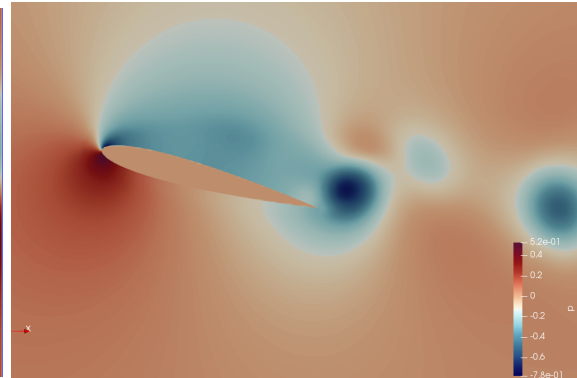


Figure 52: Pressure between maximum and minimum lift [Nm^{-2}]



Figure 53: Vorticity between maximum and minimum lift [s^{-1}]

On figure 51, 52 and 53 a vortex has clearly appeared at the trailing edge. The pressure side of the foil gets less pressure at the trailing edge which confirms that the lift is decreasing.

- At minimum lift

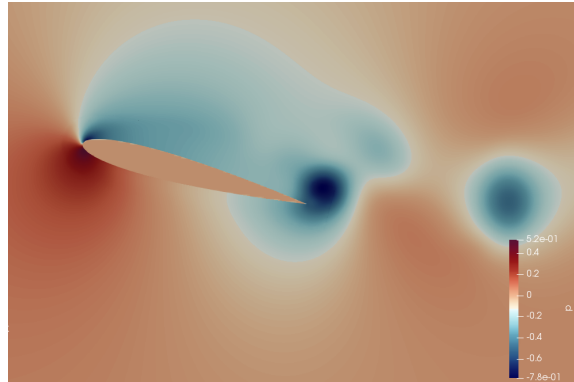
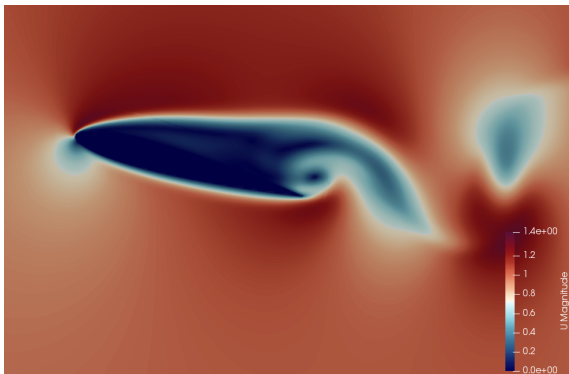


Figure 54: U magnitude for minimum lift [ms^{-1}] Figure 55: Pressure at minimum lift [Nm^{-2}]



Figure 56: Vorticity at minimum lift [s^{-1}]

In figure 54, 55 and 56 the vortex is completely developed and the pressure on the pressure side of the foil has decreased a little bit more compared to the previous figure.

9 Heaving and pitching foil

9.1 Heave and pitch equations

To make the foil imitate the motion of a subcarangiform fish the equation for the rigid body motion with the foil is divided into an equation representing the heaving and an equation representing the pitching. Heaving is described by (Lampropoulos et al. [16]):

$$y(t) = y_o \sin(\omega t) \quad (12)$$

Pitching is described by:

$$\theta(t) = \theta_0 \sin(\omega t - \psi) \quad (13)$$

ω represents the angular frequency, y_0 the heaving amplitude, θ_0 the pitching amplitude and ψ the phase lag between pitching and heaving (Lampropoulos et al. [16]).

9.1.1 Parameters for the rigid motion of the foil

The motion of a rigid foil with subcarangiform characteristics uses the following parameters. From Eloy [6] the maximum angle of attack is chosen to be 47° , the tail-beat frequency is 4 Hz [6]. Anderson et al. [12] discuss the impact of the Reynolds number on the results of the flapping foil and conclude that it is not influencing significantly the results. Therefore, the analysis will not depend on the Reynolds number. Since the static studies of the foil in this thesis have been done at $Re = 1000$ it is more reasonable to take a low Reynolds number. Inspired from Anderson et al. [12] this present study will use $Re = 1100$. From Eloy [6] the Strouhal number is taken as 0.26. The amplitude of the heaving is taken from Anderson et al. [12] as $\frac{h}{c} = 0.75$. Where c is the chord length and h the amplitude of the heaving. Since the chord length is 1 m in our case h is equal to 0.75 m. Then the flow velocity needs to be defined. From the Strouhal number $St = \frac{fA}{U}$ the velocity U is equal to 23.08 ms^{-1} . Where A is taken as $2 \cdot h = 1.5 \text{ m}$. All these parameters can then be inserted in the heaving and pitching equations.

9.1.2 Calculation of thrust produced

From Anderson et al. [12] the thrust can be calculated with equation 14.

$$T = \rho \int_a^b u(y)(u(y) - U) dy \quad (14)$$

Where U is the velocity far away from the foil. $u(y)$ is the velocity in the wake of the foil as a function of the height y of the domain. Equation 14 is integrated along the outlet 30 times within one period of oscillation. For $\psi = 90^\circ$, $T = 4138943 \text{ N}$. This means that this motion is producing

thrust. The vorticity during one period of tail-beat can be seen in the next section. For $\psi = 10^\circ$, $T = 17726777$ N. The thrust has been calculated assuming that the boundary were far away with a velocity like the inflow velocity. This assumption is not correct and the positive thrust does not correspond to the flow features as it can be seen in the next section.

9.2 Vorticity during one period for $\psi = 90$

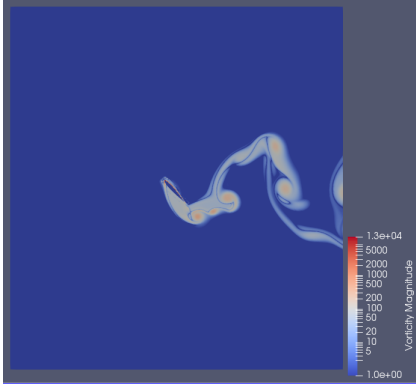


Figure 57: $t = 3$ s

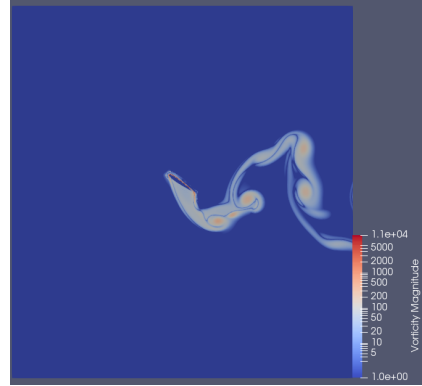


Figure 58: $t = 3.0248$ s

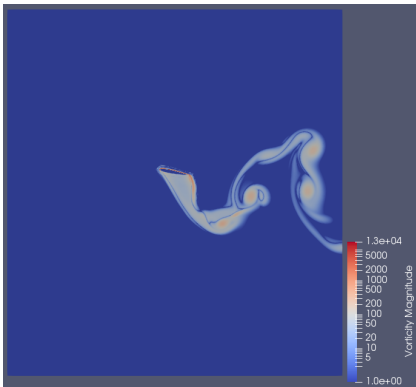


Figure 59: $t = 3.05$ s

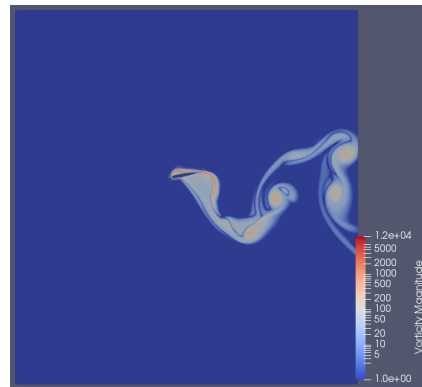


Figure 60: $t = 3.0748$ s

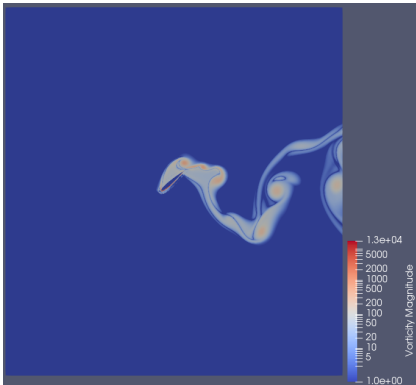


Figure 61: $t = 3.108$ s

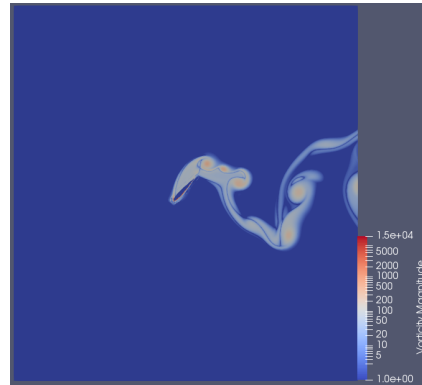


Figure 62: $t = 3.1244$ s

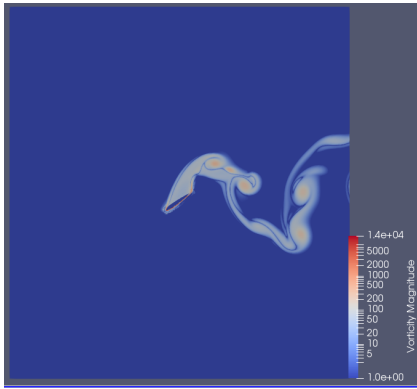


Figure 63: $t = 3.1496$ s

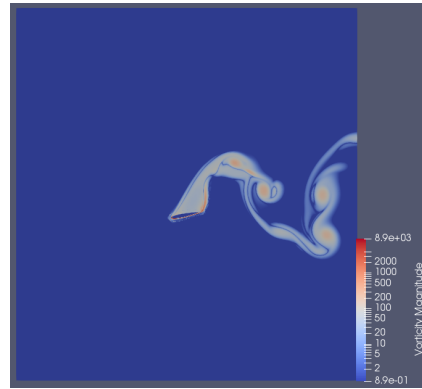


Figure 64: $t = 3.1744$ s

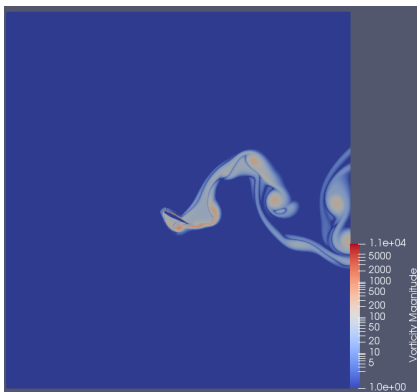


Figure 65: $t = 3.216$ s

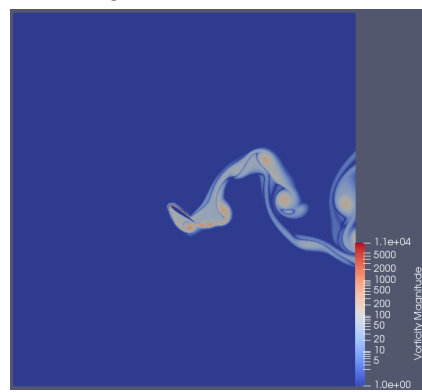


Figure 66: $t = 3.224$ s

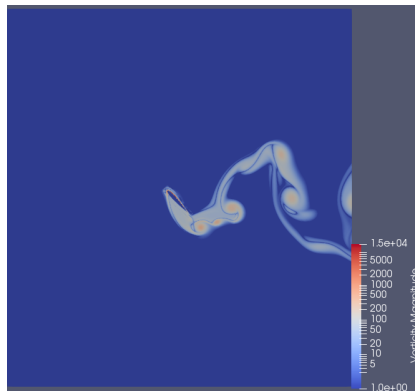


Figure 67: $t = 3.2492$ s

9.3 Vorticity during one period for $\psi = 10$

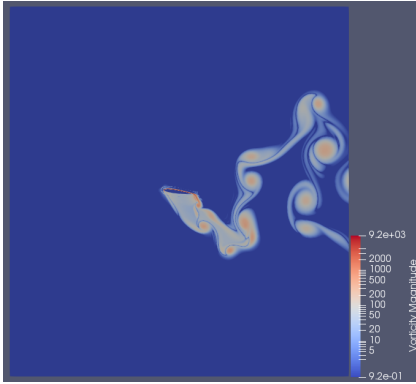


Figure 68: $t = 3$ s

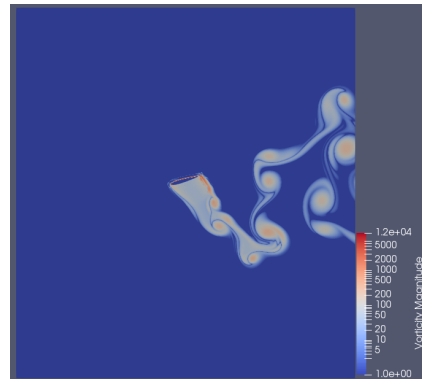


Figure 69: $t = 3.0248$ s

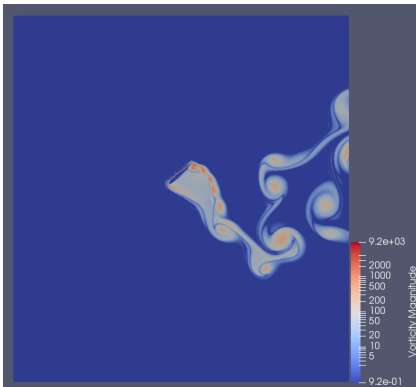


Figure 70: $t = 3.05$ s

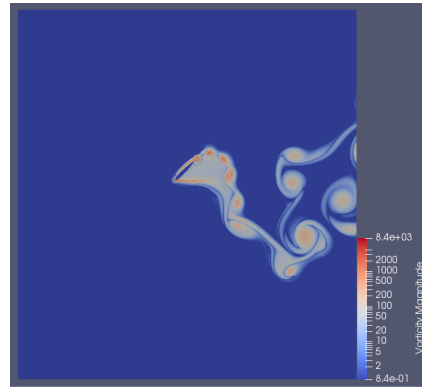


Figure 71: $t = 3.0748$ s

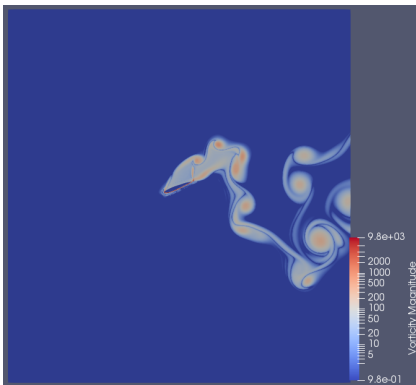


Figure 72: $t = 3.108$ s

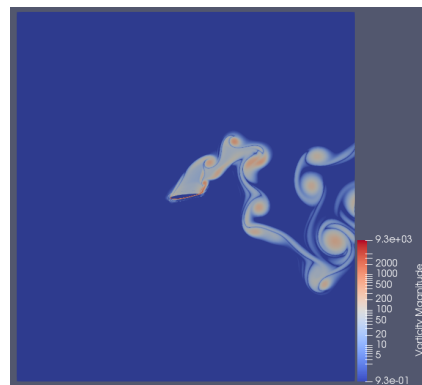


Figure 73: $t = 3.1244$ s

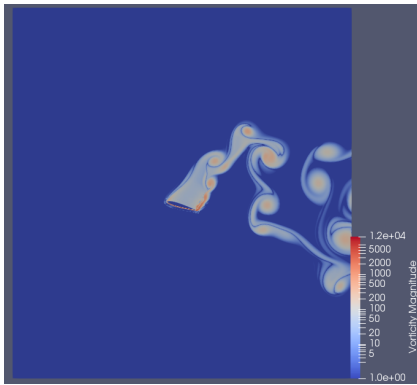


Figure 74: $t = 3.1496$ s

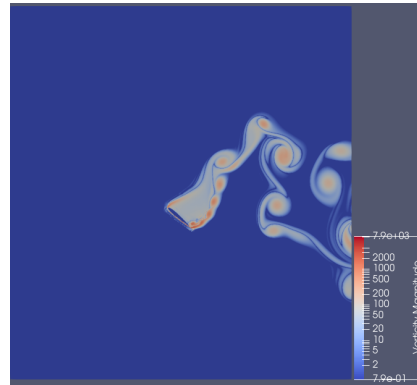


Figure 75: $t = 3.1744$ s

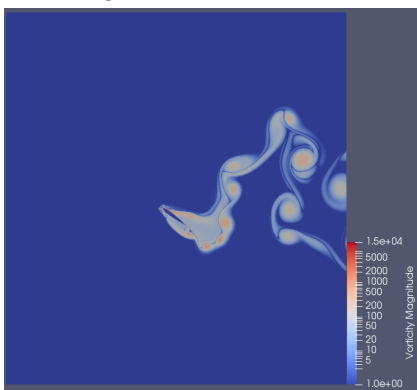


Figure 76: $t = 3.216$ s

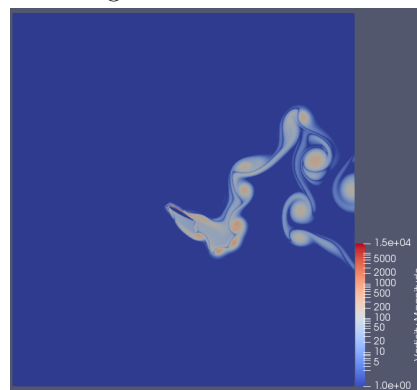


Figure 77: $t = 3.224$ s

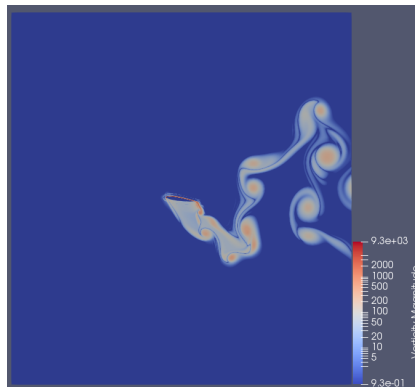


Figure 78: $t = 3.2492$ s

9.4 Drag coefficient on the body

- $\psi = 90$

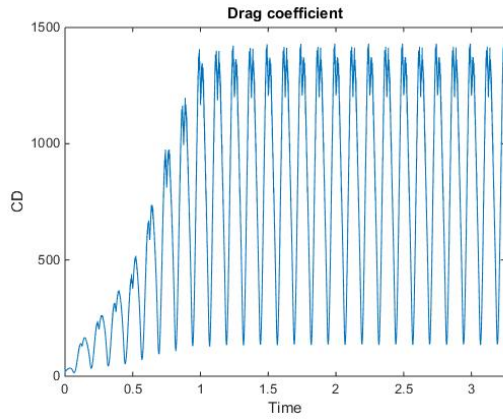


Figure 79: Drag coefficient for $\psi = 90$

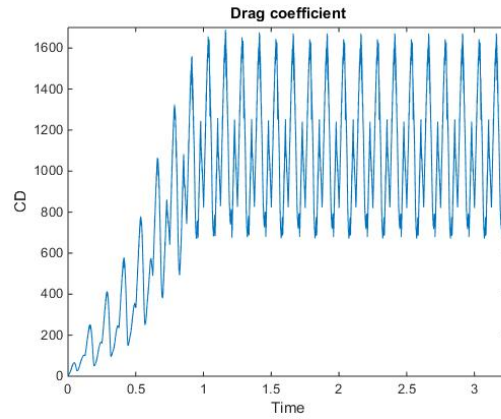


Figure 80: Drag coefficient for $\psi = 10$

In figure 79 the drag is positive, this means that the drag force is in the direction of the outlet. The drag coefficient is consistent with the pictures from the vorticity which are showing a BvK vortex street.

Figure 80 shows also that the motion of the foil is producing drag. This is also consistent with the pictures from the vorticity for $\psi = 10$.

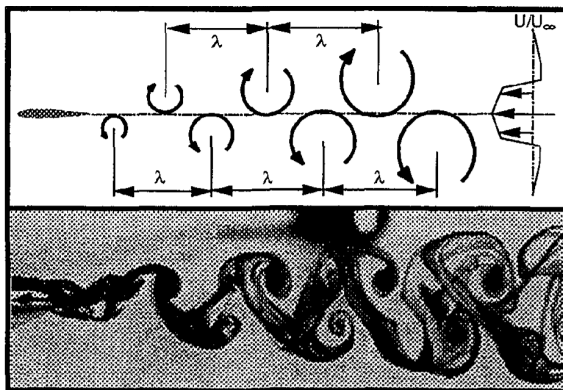


Figure 81: Drag producing vortex
Picture taken from Jones et al. [13]

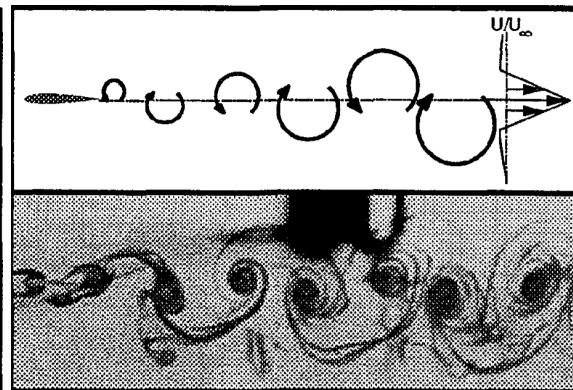


Figure 82: Thrust producing vortex
Picture taken from Jones et al. [13]

Figure 81 and 82 show respectively the vortices induced by drag and thrust (Jones et al. [13]). In both cases ran in Openfoam the vorticity is showing vortices induced by drag like figure 81. For drag producing vortex, the vortices above the foil are rotating clockwise whereas the vortices below

are rotating counter clockwise. For thrust producing vortex the opposite is happening. In Openfoam it can be seen that the vortices are rotating like in figure 81.

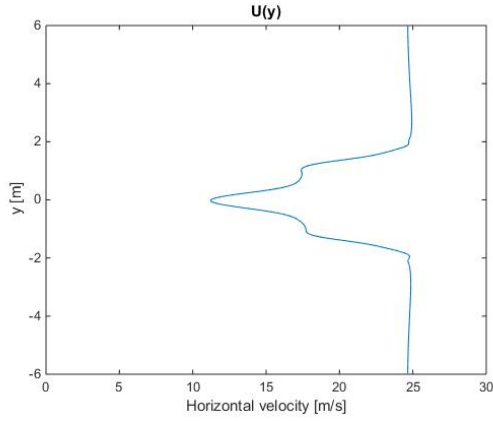


Figure 83: Velocity profile behind the foil for $\psi = 90^\circ$

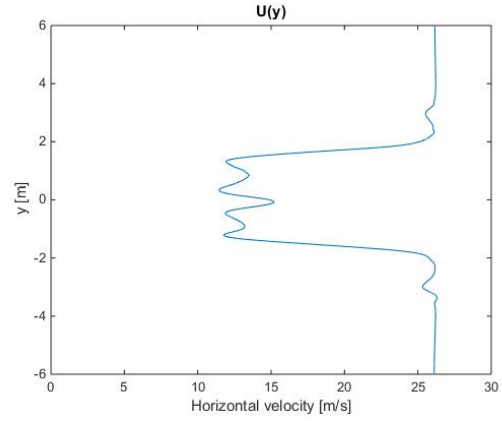
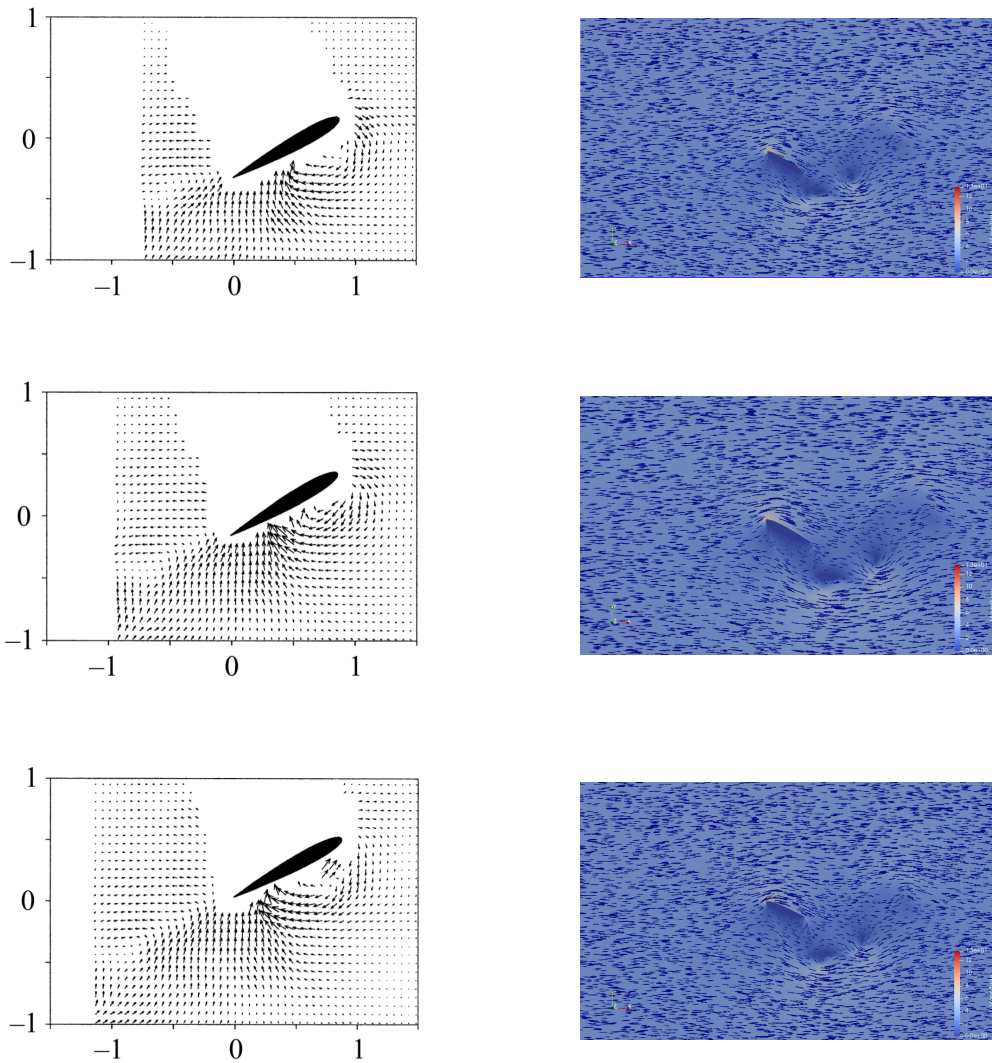


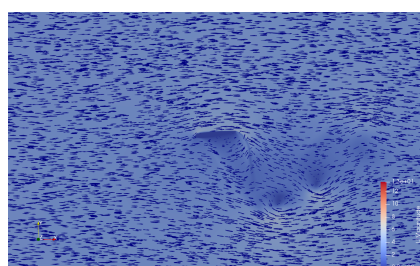
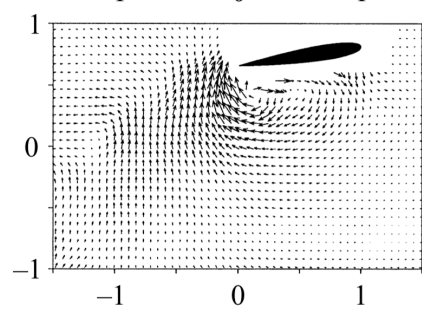
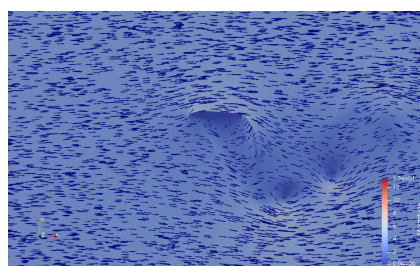
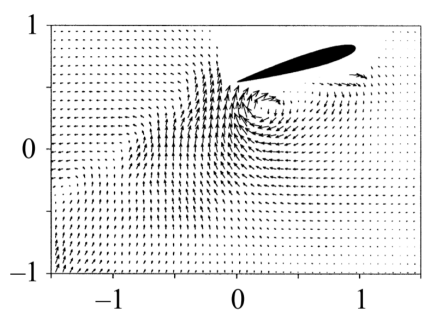
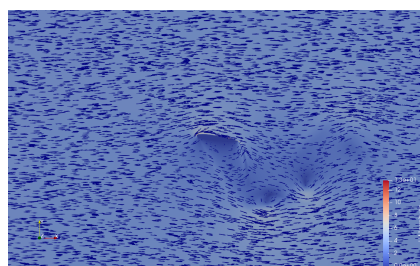
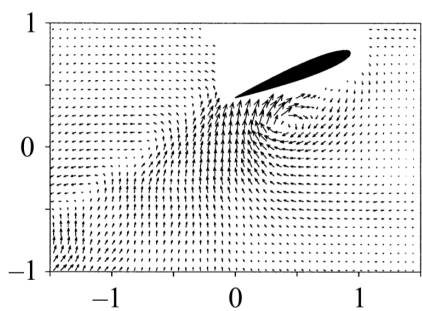
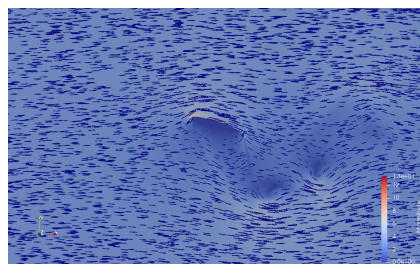
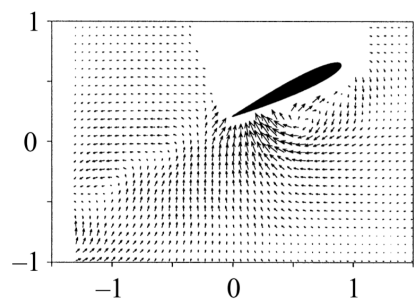
Figure 84: Velocity profile behind the foil for $\psi = 10^\circ$

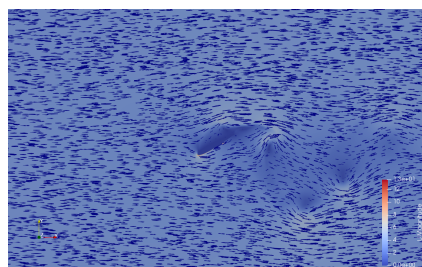
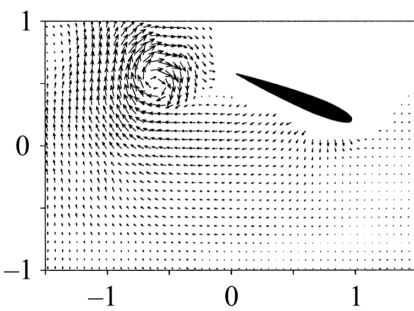
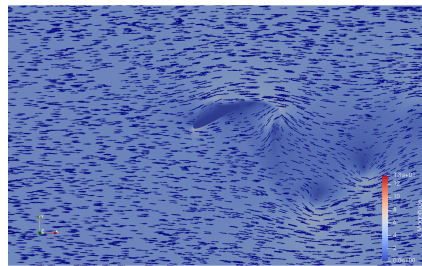
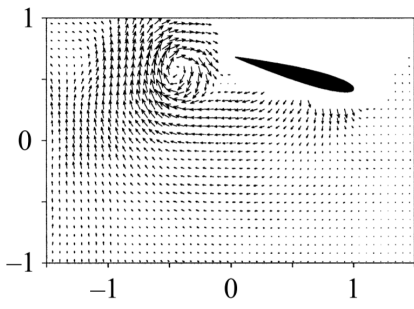
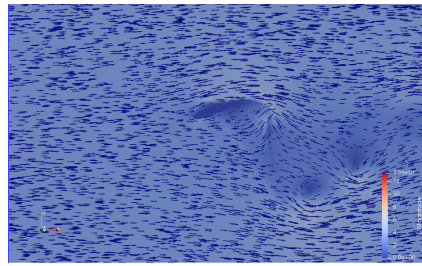
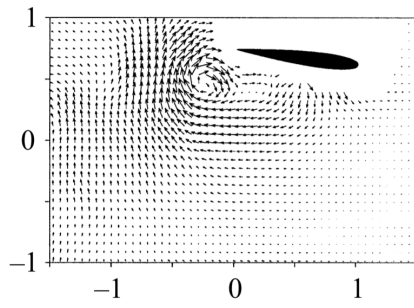
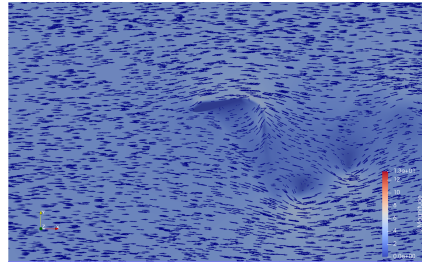
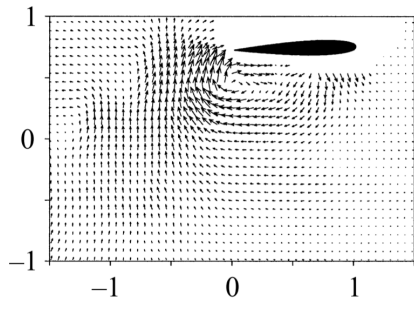
Figure 83 and 84 show the velocity profile in the wake behind the foil for $\psi = 90^\circ$ and $\psi = 10^\circ$. For both cases the velocity is decreased in the middle of the height behind the foil. This corresponds more to figure 81 from Jones et al. [13]. This is consistent with the screenshots of the vorticity and the drag coefficient.

9.5 Comparison of velocity field with Anderson et al.

The following figures compare the velocity field between Anderson et al. [12] (left) and Openfoam (right). The twelve figures show the foil for a non-dimensional half period with non dimensional time step equal to 0.042. The pictures at left are taken from Anderson et al. [12]. The start time taken from Openfoam may be slightly different from Anderson et al. The difference on each time step is quite clear. The velocity field from Anderson et al. on the pressure side of the foil shows a tendency to be directed perpendicularly against the surface of the foil. On the figures from Openfoam the velocity field is more streamlined and the vectors are almost parallel to the foil.







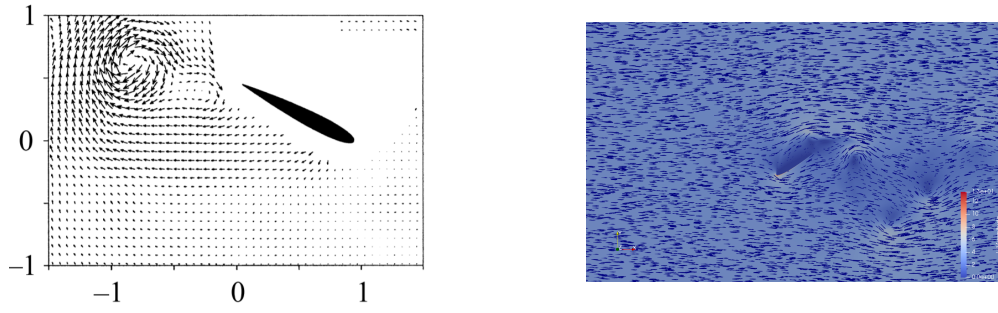


Figure 85: Velocity field at left taken from Anderson et al. [12] and Openfoam (right). The pictures are taken from one half period with dimensionless time step $\Delta t = 0.042$

9.6 Pitching foil

In the previous section the heaving and pitching foil didn't give expected thrust but drag. In order to find about the issue in Openfoam it is necessary to make simpler simulations. A simulation with a pitching foil with parameters like in the paper from Godoy-Diana [10] is done in this section. The Reynolds number is 1173, the Strouhal number is 0.22 and the amplitude of oscillation is 0.2124 m. The vorticity and velocity field is compared against Godoy-Diana et al. [10].

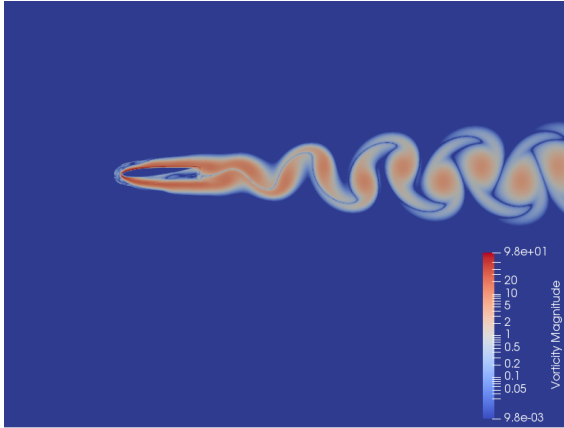


Figure 86: Screenshot from the vorticity at $t = 9.9365$ s

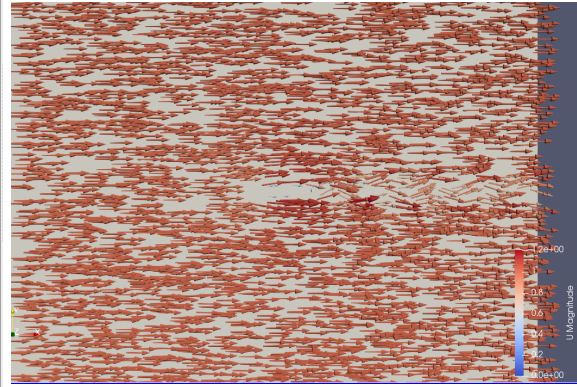


Figure 87: Velocity field from the entire domain at $t = 9.9365$ s

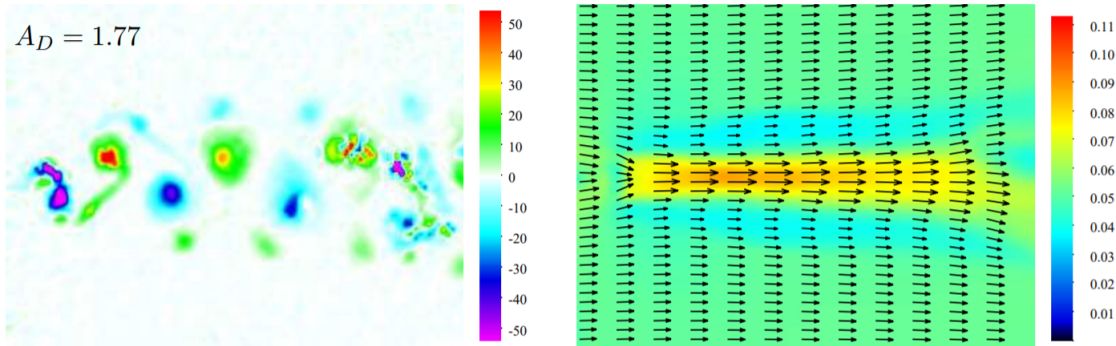


Figure 88: Spanwise vorticity (left) and mean flow (right) from Godoy-Diana et al. Picture taken from Godoy-Diana [10]

The vorticity shown in figure 86 in Openfoam seems to behave like a BvK vortex street and the velocity field at the outlet doesn't converge to the middle like in figure 88.

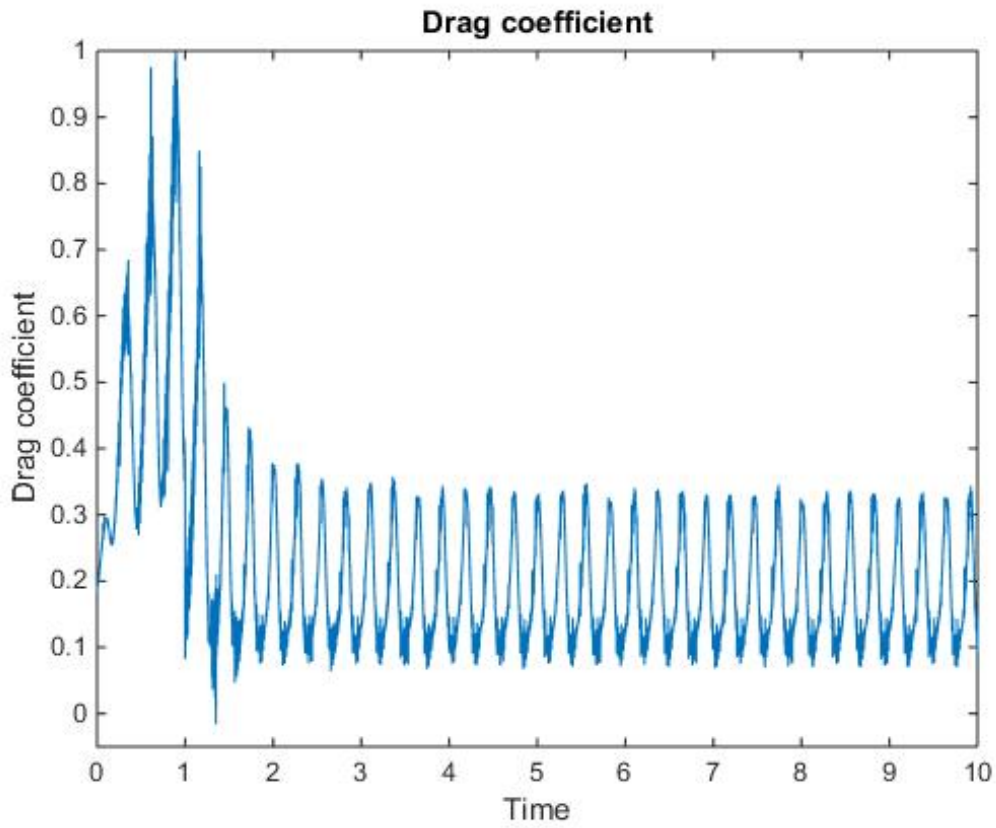


Figure 89: Drag coefficient for the flapping foil

Figure 89 shows that the drag is positive but close to zero. This is consistent with the vorticity and shows that this motion is not producing thrust as it is expected.

These investigations suggest that the overset grid used in this study is not optimal. The body-fitted grid may be too small and it is suggested that the use of one or several refinement grids is necessary.

10 Discussion and further work

The results for the simulation of a static NACA0012 foil at low Reynolds number (1000) have shown very satisfying results compared to the literature with results from Kurtulus [14] and Baradazzi, Lugni (preliminary results, personal communication). But some improvements are still possible. In the boundary between the bodyfitted grid and the background grid a small discontinuity was visible. Since the results agreed well with the literature this was neglected in this case. In further investigations the cell size at the boundary grid should be better adjusted. Notice that the use of two grids is very disadvantageous because of the very high number of cells and thus a very long running time for the simulations. To improve the grid quality and decrease the running time the use of several refinement grids should be possible. Remind that the use of three grids made a discontinuity appear between the bodyfitted grid and the refinement grid. Investigations about Openfoam and the use of decomposition in the supercomputer should be done in order to solve this issue.

The results about the heaving and pitching foil didn't give expected results. Both cases were subjected to drag. The case with a phase angle $\psi = 90$ was expected to produce thrust but it created drag instead. The case for $\psi = 10$ was expected to produce very low thrust or drag and produced drag. These expectations are based on the findings from Anderson et al. [12] showing that the phase angle is crucial to obtain thrust. A simulation with a pitching foil was also tested but didn't neither give satisfying results compared to Gody-Diana et al. [10]. The results suggest that the model used in Openfoam is not optimal and the use of one or several refinement grids could possibly give better results. But since this was not working when using the supercomputer, the reason of this issue should be investigated. An other possibility could be to make a much wider bodyfitted grid using an unstructured meshing. The cells near the foil should be much finer than in the previous simulations and be expanded until the boundary of the bodyfitted grid. The cell size of the background grid could then be bigger and the running time could be reduced.

Once the right grid for the motion is decided, the study should be continued with a flexible body using the equation of motion of a subcarangiform fish. The study could then be extended to a 3D study. Furthermore, the study does not take account for the fins a fish uses for the propulsion. The motion of the fins and their role should be studied and included in the simulations. During all the stages of these studies numerical results should be compared with experimental results if available. The flexible body motion has not yet been studied during the thesis and would be part of future investigations in Openfoam. In addition, investigations should also be done with a higher Reynolds number at turbulent flows.

11 Conclusion

During the thesis a static study with a NACA0012 foil has been done in order to validate a grid that will be used for the rigid motion simulations. The first strategy used a rectangular grid with the foil at $AOA = 0^\circ$ made in ICEM where the points composing the foil were rotated in Openfoam. This grid with moved points was then simulated for $Re = 5000$ at several angles of attack and compared with the literature. This model was then rejected since it didn't give good results. Next a overset grid strategy was tested in Openfoam with three different grids. One for the foil, one as a refinement grid and one last as a background grid. Simulations were run for $Re = 5000$ and $Re = 1000$. The use of three grids was thought to make the cell size increase smoothly and reduce the number of cells as much as possible. Paraview showed that the use of three grids for the overset strategy made some discontinuity appear between the bodyfitted grid and the refinement grid. Several tests showed that using only two grids made this discontinuity disappear. It seems from these results that the supercomputer had some issues when reconstructing the results from the decomposing in different processors. The final convergence study was then conducted with two grids in Openfoam for $Re = 1000$ for $AOA = 15^\circ$. This has the drawback to have the same cell size on the entire domain and increases considerably the running time on the supercomputer. In order to have reasonable running time for the rigid body motion a compromise between running time and accuracy of results was made to choose the grid. The final step was to make the foil imitate the subcarangiform motion with a rigid body. The parameters of the subcarangiform motion were inserted in the equation of heave and pitch. Two phase angles were then tested for the motion, one which was expected to give thrust ($\psi = 90^\circ$) based on the study of Anderson et al. [12] and one which was expected to give drag or less thrust ($\psi = 10^\circ$). The drag coefficient in both cases was positive where positive x is in the direction of the outlet, which means that both cases were producing drag. The velocity profile in both cases shows that the velocity is decreased in the wake area, this confirms that drag is created by the foil. The screenshots of the vorticity during one period for both cases show a BvK vortex street. This is consistent with the drag coefficient and the velocity profile behind the foil. The study didn't show expected results for the heaving and pitching foil at $Re = 1100$ and further investigations should be made on a wider range of Reynolds number and larger domain size to see the impact on the drag force. Finally, a last investigation on a pitching foil was made. The model was tested with the grid chosen from the convergence study. The simulation gave thrust and BvK vortex street. The results suggest that the model used during these simulations works for static cases but not for motion cases. The reason could be that the bodyfitted grid is too coarse and not large enough. This means that the use of one or several refinement grids would possibly give better results. But, since the use of three grids in overset didn't work with the use of decomposition in the supercomputer, this shows the limits of Openfoam. The next investigation should be done with a bodyfitted grid that is much wider and finer around the foil using unstructured cells. The cells should be very fine near the foil and expanded until the boundary of the bodyfitted grid which would allow to use a bigger cell size for the background grid and then reduce the running time.

References

- [1] Openfoam tutorial guide. <https://www.openfoam.com/documentation/tutorial-guide/>. Accessed: 2018-09-30.
- [2] ARCHER, S. D., AND JOHNSTON, I. A. Kinematics of labriform and subcarangiform swimming in the antarctic fish *nothothenia neglecta*. *Journal of Experimental Biology* 143 (1989), 195–210.
- [3] AUDREY P. MAERTENS, A. G., AND TRIANTAFYLLOU, M. S. Optimal undulatory swimming for a single fish-like body and a pair of interacting swimmers. *Journal of Fluid Mechanics* 813 (2017), 1087–1101.
- [4] ÇENGEL, Y. *Fluid Mechanics*. Çengel series in engineering thermal-fluid sciences. Tata McGraw Hill Education Private, 2010.
- [5] DR. DAVID M. LANE, MICHAEL SFAKIOTAKIS, D. J. B. C. D. Review of fish swimming modes for aquatic locomotion. *IEEE Journal of Oceanic Engineering* 24 (1999), 237–252.
- [6] ELOY, C. Optimal strouhal number for swimming animals. *Journal of Fluids and Structures* 30 (2012), 205–218.
- [7] ESMAEIL ESMAELIFARA, MOHAMMAD HASSAN DJAVARESHKIANA, B. F. F. A. E. Hydrodynamic simulation of an oscillating hydrofoil near free surface in critical unsteady parameter. *Ocean Engineering* 141 (2017), 227–236.
- [8] FALTINSEN, O. M. *Hydrodynamics of High-Speed Marine Vehicles*. Cambridge University Press, New York, 2005.
- [9] G. COLICCHIO, M. GRECO, O. M. F. A bem-level set domain-decomposition strategy for non-linear and fragmented interfacial flows. *International journal for numerical methods in engineering*. 67 (March 2006), 1385–1419.
- [10] GODOY-DIANA, R., AIDER, J.-L., AND WESFREID, J. E. Transitions in the wake of a flapping foil. *Phys. Rev. E* 77 (Jan 2008), 016308.
- [11] I. BORAZJANI, F. S. On the role of form and kinematics on the hydrodynamics of self-propelled body/caudal fin swimming. *Journal of Experimental Biology* 213, 1 (2009), 9–107.
- [12] J. M. ANDERSON, K. STREITLIEN, D. S. B. M. S. T. Oscillating foils of high propulsive efficiency. *Journal of Fluid Mechanics* 360 (1997), 41–72.
- [13] JONES, K. D., AND PLATZER., M. F. Numerical computation of flapping-wing propulsion and power extraction.

- [14] KURTULUS, D. F. On the unsteady behavior of the flow around naca 0012 airfoil with steady external conditions at $re=1000$. *International journal of micro air vehicles Volume: 7 issue: 3* (2015), 301–326.
- [15] L. SCHOUVEILER, F.S. HOVER, M. T. Performance of flapping foil propulsion. *Journal of Fluids and Structures* (2005).
- [16] NIKOLAOS LAMPROPOULOS, D. K., AND BELIBASSAKIS, K. Numerical simulation of flapping foil propulsion.
- [17] RAZAVI, S. E., AND ORANG, A. A. A comparative investigation of hydrofoil at angles of attack. *International Journal for Numerical Methods in Fluids 68* (2011), 1087–1101.
- [18] SCHULTZ, W. W., AND WEBB, P. W. Power requirements of swimming: Do new methods resolve old questions? *INTEGR. COMP. BIOL 42* (2002), 1018–1025.
- [19] Z. CUI, Z. YANG, L. S. H. J. Complex modal analysis of the movements of swimming fish propelled by body and/or caudal fin. *Wave Motion 78* (2018), 83–97.